
Dissecting Self-Supervised Learning Methods for Surgical Computer Vision

Sanat Ramesh^{a,c,1,*}, Vinkle Srivastav^{a,1}, Deepak Alapatt^{a,1}, Tong Yu^{a,1}, Aditya Murali^a, Luca Sestini^{a,d}, Chinedu Innocent Nwoye^a, Idris Hamoud^a, Antoine Fleurentin^b, Georgios Exarchakis^{a,b}, Alexandros Karargyris^{a,b}, Nicolas Padoy^{a,b}

^aICube, University of Strasbourg, CNRS, Strasbourg 67000, France

^bIHU Strasbourg, Strasbourg 67000, France

^cAltair Robotics Lab, Department of Computer Science, University of Verona, Verona 37134, Italy

^dDepartment of Electronics, Information and Bioengineering, Politecnico di Milano, Milano 20133, Italy

Abstract: The field of surgical computer vision has undergone considerable breakthroughs in recent years with the rising popularity of deep neural network-based methods. However, standard fully-supervised approaches for training such models require vast amounts of annotated data, imposing a prohibitively high cost; especially in the clinical domain. Self-Supervised Learning (SSL) methods, which have begun to gain traction in the general computer vision community, represent a potential solution to these annotation costs, allowing to learn useful representations from only unlabeled data. Still, the effectiveness of SSL methods in more complex and impactful domains, such as medicine and surgery, remains limited and unexplored. In this work, we address this critical need by investigating four state-of-the-art SSL methods (MoCo v2, SimCLR, DINO, SwAV) in the context of surgical computer vision. We present an extensive analysis of the performance of these methods on the Cholec80 dataset for two fundamental and popular tasks in surgical context understanding, phase recognition and tool presence detection. We examine their parameterization, then their behavior with respect to training data quantities in semi-supervised settings. Correct transfer of these methods to surgery, as described and conducted in this work, leads to substantial performance gains over generic uses of SSL - up to 7% on phase recognition and 20% on tool presence detection - as well as state-of-the-art semi-supervised phase recognition approaches by up to 14%. The code will be made available at <https://github.com/CAMMA-public/SelfSupSurg>.

Keywords: Self-supervised learning; Semi-supervised learning; Surgical computer vision; Deep learning; Endoscopic videos; Laparoscopic cholecystectomy

1. Introduction

Automatic analysis and interpretation of visual signals from the operating room (OR) is the primary concern of surgical computer vision, a fast-growing discipline that is expected to play a major role in the development of reliable decision support systems for surgeons (Maier-Hein et al., 2017). Recent developments in the field have indeed resulted in increasingly refined vision algorithms; however, a majority of these studies have only been conducted on datasets containing small amounts of recorded procedures, all of which have been manually annotated by clinical experts. In future developments, much larger quantities of data will be required in order to account for variations in anatomy, patient demographics, clinical workflow, surgical skills, instrumentation and image acquisition (Maier-Hein et al., 2022).

For that purpose, raw video data can be supplied on a very large scale by laparoscopic surgeries, since they are guided by intra-abdominal video streams: in the United States, nearly 1M laparoscopic cholecystectomies are performed each year,

resulting in approximately 630k hours of footage for just this one type of procedure. Yet, datasets used for training current surgical vision models remain disproportionately small. For example, Cholec80 (Twinanda et al., 2016b), one of the most popular datasets in the field (Maier-Hein et al., 2017), hardly exceeds 50 hours of recordings. Apart from medico-legal constraints, the critical factor leading to this sparsity of data is the reliance on manual annotations. While labels for natural images can be easily supplied by the general public, surgical annotations usually require clinical expertise. As a result, the fully supervised approach - i.e. training models with entirely annotated datasets - may prove to be unsustainable in surgical computer vision.

In computer vision, an alternative has emerged in the form of Self-Supervised Learning (SSL) (Jing and Tian, 2021). Considerable progress has been made in this area, with increasingly refined methods for extracting rich vector representations from images without labels, using only the raw pixel data. This research topic has so far not been thoroughly explored in surgical applications. In the few self-supervised training tasks proposed by the community, learning from the visual content itself is generally de-emphasized in favor of utilizing other available sources of information - for example time (Funke et al., 2018; Yengera et al., 2018), stereoscopy (Yang and Kahrs, 2021) or robot kinematics (Sestini et al.,

*Corresponding author: Tel.: +33-039-041-3553;

e-mail: sanat.ramesh@univr.it (Sanat Ramesh)

¹Sanat Ramesh, Vinkle Srivastav, Deepak Alapatt and Tong Yu contributed equally and share co-first authorship.

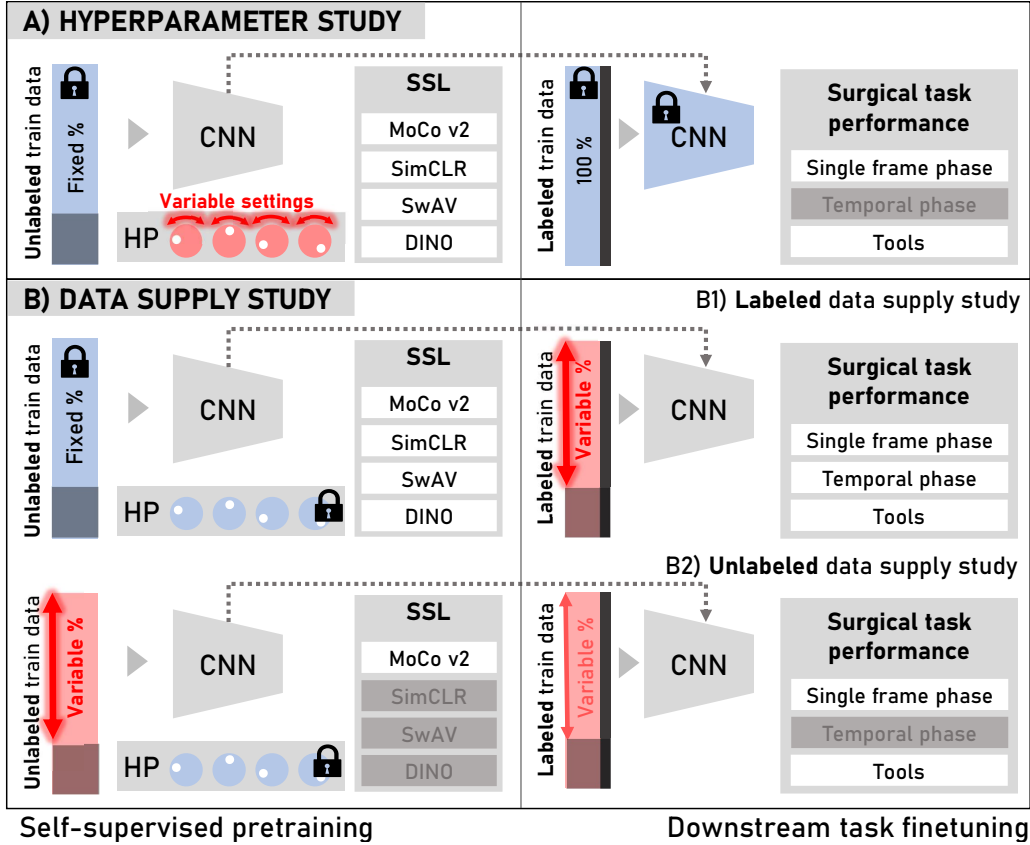


Fig. 1. Two stages of the study: (A) Hyperparameter study: Analyzing the influence of hyperparameters when adapting SSL methods to the surgical domain. (B) Data supply study: Evaluating the response of SSL methods to varying amounts of (1) labeled and (2) unlabeled data.

2021). State-of-the-art natural image SSL methods, with their advanced representational capabilities, have yet to be adequately demonstrated on surgical images.

However expanding SSL methods outside of natural images can be challenging, especially in a complex domain such as surgery. Most notably, heavy parameter tuning based on heuristics (Xiao et al., 2020) might be required. Robustness against large variations in domains and tasks also is not guaranteed; in-depth performance analysis has essentially been conducted on general computer vision datasets (Feichtenhofer et al., 2021a), most commonly Imagenet, which contains 14M images and over 1000 visually distinct classes. In contrast, Cholec80, one of the most prominent surgical computer vision datasets (Maier-Hein et al., 2017), contains 80 videos of procedures resulting in under 200k frames at 1fps. Only 7 classes of surgical phases and 7 classes of tools are featured; moreover, the visual evidence to distinguish them is highly sparse, especially for time-based tasks such as surgical phase recognition, a coarse-grained form of activity recognition. Further, since surgical videos can last up to several hours depicting a relatively stable scene, it is non-trivial to determine how existing SSL frameworks can best accommodate frames coming from the same procedure. Finally, these issues may be exacerbated by surgery-specific confounding factors such as smoke, bleeding, occlusions, or rapid tool movements. Such fundamental differences between natural and surgical image data motivate the need for a thorough study of SSL in the

surgical domain.

The work presented here thoroughly addresses this need in two distinct steps (see Fig. 1). We select four SSL methods - MoCo v2 (Chen et al., 2020b), SimCLR (Chen et al., 2020a), SwAV (Caron et al., 2020), DINO (Caron et al., 2021) - suitably covering the state of the art in general computer vision, and extensively examine hyperparameter variations for each of them on Cholec80. We identify key differences with the natural image domain, highlighting hyperparameter tuning as a non-trivial and crucial element of SSL method transfer. In the second step, we set hyperparameters to their optimal values and test out the quality of the representations learned through each of these methods on two classic surgical downstream tasks: phase recognition and tool presence detection. We finally verify how these approaches respond to varying amounts of labeled and unlabeled data in a practical semi-supervised setting. Here, we show that these methods, while generic in design, achieve state-of-the-art performance for both tasks and significantly mitigate the reliance on annotated data, adding up to 7% phase recognition F_1 score and 20.4% tool presence detection mAP.

This paper’s contributions are as follows:

1. Benchmarking of four state-of-the-art self-supervised learning methods (MoCo v2 (Chen et al., 2020b), SimCLR (Chen et al., 2020a), SwAV (Caron et al., 2020), and DINO (Caron et al., 2021)) in the surgical domain.

2. Thorough experimentation (~ 200 experiments, 7000 GPU hours) and analysis of different design settings - data augmentations, batch size, training duration, frame rate and initialization - highlighting a need for and intuitions towards designing principled approaches for domain transfer of SSL methods.
3. In-depth analysis on the adaptation of these methods, originally developed using other datasets and tasks, to the surgical domain with a comprehensive set of evaluation protocols based on surgical tasks.
4. Extensive evaluation (~ 280 experiments, 2000 GPU hours) of the scalability of these methods to various amounts of labeled and unlabeled data through an exploration of both fully and semi-supervised settings.

2. Related Work

2.1. Self-supervised representation learning in general computer vision

In the absence of external labels, SSL methods rely on the input image’s intrinsic information to define a proxy loss to minimize. This artificial loss forces the model to learn rich vector representations of images, i.e. vectors in an embedding space with relative positions that meaningfully reflect the original visual content. The underlying expectation is that these representations are suitable for a wide range of useful downstream tasks.

The following paragraphs provide an overview of the various categories of SSL methods, tracing their evolution over the past few years.

Heuristics-based methods. Early SSL approaches aimed to learn representations by training models to solve a simple handcrafted task with some degree of relevance to the target task (Kim et al., 2018). These included predicting spatial context (Doersch et al., 2015), image rotation (Gidaris et al., 2018), artificial classes based on geometric transformations (Dosovitskiy et al., 2014a), and image patch arrangement (Noroozi and Favaro, 2016). Similarly, other works proposed reconstructing image regions (Pathak et al., 2016) or colorization (Zhang et al., 2016, 2017). Jing et. al. provide an exhaustive review of pretext-task based SSL methods in (Jing and Tian, 2020).

Contrastive methods. More recently, contrastive learning methods have emerged as an alternative to handcrafted heuristics. These methods place less emphasis on the nature of the pretext task, instead focusing on controlling the relative position of features in the embedding space. They rely on generating positive and negative pairs of samples, which are then passed to a discriminative loss function to generate a training signal.

Early works attempted to generate such samples from within a single image using image patches (Dosovitskiy et al., 2014b; Oord et al., 2018); however, these methods failed to take advantage of relationships between different images. Consequently, Wu et al. (2018) proposed the concept of a memory bank to store representations of many instances, which they leverage to impose an inter-instance discrimination

objective. He et al. (2020) refined this idea with MoCo, using a momentum encoder rather than a memory bank to store representations, thereby enabling the sampling of many more instance pairs for the discrimination objective. An improved version with an additional projection head and more augmentations, MoCo v2, was later proposed by Chen et al. (2020b). Recently, Chen et al. (2020a) introduced SimCLR, a simpler framework outperforming many previous works (Oord et al., 2018; Bachman et al., 2019; Henaff, 2020; Tian et al., 2020; Misra and Maaten, 2020) by using aggressive data augmentations to generate ‘positive pairs’ for the discrimination objective.

Cluster-based and distillation-based methods. While contrastive methods have brought significant performance improvements, requiring positive and negative sampling during training can be impractical, and has pushed the community towards alternative approaches.

Self-supervised clustering methods (Caron et al., 2018; Asano et al., 2019; Caron et al., 2020; Grill et al., 2020a; Caron et al., 2021) provide another alternative to the pretext task-based approach, focusing on clustering latent image representations in embedding space. Initially, Caron et. al. introduced DEEPCUSTER (Caron et al., 2018), which adapted the k-means algorithm to assign clusters to images. Asano et al. (2019) showed reformulating cluster assignment as an optimal transport problem improves performance. SwAV (Caron et al., 2020) further improves on this by constraining augmented views of an image to have consistent cluster assignments.

Other works, based on distillation, bootstrap multiple neural networks in a teacher-student fashion to learn latent representations (Grill et al., 2020a). DINO (Caron et al., 2021) applies this bootstrapping approach with vision transformers, attaining state-of-the-art results.

Spatio-temporal methods. Parallel to static image methods presented in the previous three paragraphs, research on SSL has explored video data through approaches tailored to spatio-temporal models. Most of them rely on spatio-temporal heuristics, with more emphasis on timing (Misra et al., 2016; Fernando et al., 2017; Lee et al., 2017; Xu et al., 2019; Wang et al., 2019; Jenni et al., 2020; Benaim et al., 2020) or appearance (Vondrick et al., 2018; Ahsan et al., 2019; Pathak et al., 2017; Kim et al., 2019; Diba et al., 2019). A few contrastive methods exist as well (Qian et al., 2021; Pan et al., 2021; Han et al., 2020). Recently, a large-scale study by Feichtenhofer et al. (2021b) adapted four single-frame SSL methods Chen et al. (2020a); He et al. (2020); Grill et al. (2020b); Caron et al. (2020) to video data and compared their performance.

Position of our work. Self-Supervised Learning is an intensely active research topic, with a large number of very distinct approaches proposed in recent years. For this reason, choosing an SSL method - especially for anything other than natural image data - is a complex problem: comparisons presented in SSL works can only cover a small selection of methods. More importantly, these comparisons are mainly

conducted on natural image datasets such as the Imagenet dataset [Deng et al. \(2009\)](#); no reference point exists for surgical datasets, which are entirely different in terms of appearance. This is precisely the gap we fill with our work: we study how SSL adapts to surgical computer vision using a choice of methods that sufficiently span the state-of-the-art for static images. Spatio-temporal models, while potentially relevant for future studies, are omitted here due to challenging and radically different temporal modeling requirements in the surgical domain: commonly used natural video datasets in SSL ([Carreira and Zisserman, 2017](#); [Soomro et al., 2012](#); [Kuehne et al., 2011](#)) contain short clips of a single action, contrasting heavily with full recordings of surgical interventions.

2.2. Surgical computer vision.

General computer vision focuses on natural images with scenes and items from everyday life. In contrast, surgical computer vision aims at identifying surgical activities and objects with varying degrees of detail. Early work in the field focused on automatically recognizing surgical workflow at the coarsest level through two fundamental tasks: phase recognition and tool presence detection. These highly specialized visual tasks prompted developments in terms of methodology separately from the rest of computer vision, which we cover in the next paragraphs.

Full supervision. Initial efforts in surgical computer vision involved phase recognition based on handcrafted features [Padoy et al. \(2012\)](#); [Blum et al. \(2010\)](#). Deep learning was first introduced to the field by [Twinanda et al. \(2016b\)](#) and [Dergachyova et al. \(2016\)](#), replacing handcrafted features with embeddings extracted by convolutional neural networks; [Twinanda et al. \(2016b\)](#) in particular introduced the *Cholec80* dataset, containing 80 videos of cholecystectomy annotated with surgical phases and tool presence labels. This dataset has since remained as one of the computer vision community’s main datasets ([Maier-Hein et al., 2017](#)), appearing in most works mentioned in this paragraph. With surgical workflow and continuity of surgical actions playing a major role in these tasks, spatio-temporal models quickly emerged, outperforming single-frame models by a wide margin. [Twinanda et al. \(2016a\)](#) employed combinations of CNNs and LSTMs for surgical phase recognition and tool presence detection. Since then, increasingly refined spatio-temporal architectures have been proposed to better model the tasks ([Jin et al., 2018, 2020](#); [Czempiel et al., 2020, 2021](#)). Outside of these examples, a more comprehensive overview of surgical phase recognition approaches is provided in a survey by [Garrow et al. \(2021\)](#). For recognizing tools in cataract surgery, [Al Hajj et al. \(2018\)](#) proposed combinations of CNNs and RNNs with boosting.

Self-supervision in surgery. Self-supervision is still in the very early stages of research within surgical computer vision. While SSL methods in general computer vision have evolved towards methods such as contrastive learning, clustering or distillation (Section 2.1), self-supervision on surgical data is still mostly limited to heuristics; for instance [Ross](#)

[et al. \(2018\)](#) uses a colorization pretext task. Furthermore, the self-supervised tasks seen in surgery generally involve external information: [da Costa Rocha et al. \(2019\)](#); [Sestini et al. \(2021\)](#) incorporate robot kinematics. [Yengera et al. \(2018\)](#) rely on remaining surgery duration estimation as the pretext task to improve surgical phase recognition on Cholec80. The only existing examples of contrastive learning add external information as well: [Bodenstedt et al. \(2017\)](#) used a frame sorting task; later, [Funke et al. \(2018\)](#) introduced a method named second order temporal coherence. In both cases, comparisons between frames are driven by time (i.e. relative positions of frames inside of a video) instead of their actual content.

Position of our work. Current research on surgical computer vision heavily leans towards fully supervised methods, which require large amounts of data to be annotated with clinical expertise. For improved scalability, a few approaches involving self-supervision have been developed. These approaches, however, heavily rely on heuristics and external information; as such, they lag behind general SSL, which has expanded to a larger spectrum of methods in recent years, all purely based on pixel data. Our work targets this deficit by bringing recently proposed SSL methods to surgery and adapting them to this particular domain. Since single-frame feature extractors play a fundamental role in state-of-the-art spatio-temporal models in surgical computer vision, examining SSL methods designed for static images is an obligatory first step, which is the focus of this study.

3. Methodology

We first establish the setting of this study by introducing the relevant surgical data and tasks, followed by our selection of SSL methods. We then outline our experiments; two major stages are defined as shown in Fig. 1, the *hyperparameter study* and the *data supply study*. Each one examines the reaction of SSL in the surgical domain to a different factor, respectively parameterization and available data quantities. Implementation details for each stage of this study are available in the supplementary material.

3.1. Surgical data & surgical tasks

Since its introduction by [Twinanda et al. \(2016b\)](#), the Cholec80 dataset has been the foundation for many studies in surgical computer vision; we therefore use it here for our SSL benchmark. This dataset contains 80 videos of complete laparoscopic cholecystectomy procedures, recorded at 25 frames per second with a resolution of 854×480 . The average video duration is 38 minutes with 16 minutes of standard deviation, indicating a high degree of heterogeneity.

The two tasks used as downstream tasks are *tool presence detection* and *surgical phase recognition*, mirroring the *object detection* and *action recognition* tasks of general computer vision, respectively.

Tool presence detection is a multi-class, multi-label classification problem aimed at identifying all the surgical tools

appearing in a given frame (Twinanda et al., 2016b; Nwoye et al., 2019; Al Hajj et al., 2018). It goes beyond image-level classification as zero, one, or several types of tools can be detected in one surgical image frame at the same time. 7 tools are featured, as described in Fig. 2.

Surgical phase recognition entails classifying every frame of a recorded surgical procedure based on the activity being performed. This is a challenging task, since important tools or anatomical parts often exit the field of view; as a result useful visual indicators for making predictions tend to be quite sparse. Each procedure is decomposed into up to 7 phases described in Fig. 3.

CHOLEC80 TOOLS			
Name	Function		Occurrences per video
Grasper	Hold or move anatomy		1282±1669
Bipolar	Coagulate, hold or move anatomy with a pair of electrodes		111±106
Hook	Dissect tissue with an electrode		1289±672
Clipper	Ligate using clips		41±31
Scissors	Perform cuts		75±48
Irrigator	Project water, aspirate fluids		123±147
Specimen bag	Carry gallbladder		143±84

Fig. 2. Tools featured in the Cholec80 dataset.

CHOLEC80 PHASES			
Name	Description		Duration
Preparation	Exposure of gallbladder by removal of surrounding tissue		1.8±1.7 min
Calot triangle dissection	Exposure of the base of the liver bed by dissecting the gallbladder neck		15.6±11.1 min
Clipping & cutting	Application of clips to the cystic duct, cutting of cystic duct		2.9±2.1 min
Gallbladder dissection	Dissection of gallbladder from the liver bed		12.2±8.9 min
Gallbladder packaging	Insertion of dissected gallbladder into specimen bag		1.6±0.8 min
Cleaning & coagulation	Coagulation of the liver bed and cleanup using the irrigator		3.0±2.6 min
Gallbladder extraction	Extraction of the gallbladder through the umbilical trocar		1.4±1.2 min

Fig. 3. Phases featured in the Cholec80 dataset.

3.2. Selected SSL methods

As shown in Section 2.1, general computer vision offers a wide range of SSL methods. In order to adequately represent

the current state of the art, we select a total of four SSL methods: two contrastive (SimCLR (Chen et al., 2020a), MoCo v2 (He et al., 2020; Chen et al., 2020b)), one distillation-based (DINO (Caron et al., 2020)), and one clustering-based (SwAV (Caron et al., 2020)), see Fig. 4.

Several studies on unsupervised visual representation have proposed approaches based on contrastive learning (Hadsell et al., 2006; Wu et al., 2018; Van den Oord et al., 2018; Hjelm et al., 2018; Zhuang et al., 2019; Henaff, 2020; Tian et al., 2020; Bachman et al., 2019), with the core idea being to maximize the representational similarity for pairs of positive samples and dissimilarity for pairs of negative samples. A key component of these methods is mining positive and negative samples in a batch without explicit labels. A common approach in these methods is, for each image, to consider its augmentations as a corresponding positive sample, and other images as corresponding negative samples. The positive and the negative samples are passed through a base encoder to obtain the corresponding positive (x , x^+) and negative (x^-) embeddings. The InfoNCE loss (Oord et al., 2018) commonly used in contrastive methods is defined as follows:

$$L_{contrastive} = \mathbb{E}_{x, x^+, x^-} \left[-\log \frac{e^{x \cdot x^+ / \tau}}{e^{x \cdot x^+ / \tau} + \sum_{k=1}^K e^{x \cdot x^- / \tau}} \right], \quad (1)$$

where τ is a temperature hyperparameter for scaling the embeddings. The negative samples are required in contrastive methods to avoid model collapse to an identity solution. Each of the following four selected SSL methods works on similar principles with a few modifications.

SimCLR (Chen et al., 2020a) considers the other images from a batch as negative samples and passes them through the encoder to obtain the negative embeddings (x^-) to compute the contrastive loss, $L_{contrastive}$, using equation (1).

MoCo v2 He et al. (2020) introduced MoCo, employing a large memory queue to store negative embeddings x^- . This queue allows decoupling the dictionary size from the mini-batch size, in order to perform well even with smaller batch sizes. Furthermore, since the queue contains embeddings from different mini-batches, a momentum encoder is used to enforce consistency across different mini-batches. The weights of the momentum encoder (θ_m) are updated using an exponential moving average (EMA) of the weights of the encoder (θ): $\theta_m = \lambda \theta_m + (1 - \lambda) \theta$, where λ is a decay parameter. MoCo v2 (Chen et al., 2020b) refines this design using an additional projection head and more augmentations.

DINO (Caron et al., 2021), inspired by BYOL (Grill et al., 2020b), uses a teacher-student approach in a knowledge-distillation framework (Hinton et al., 2015). The student encoder, parameterized by θ_s , and the teacher encoder, parameterized by θ_t , are used to generate two positive embeddings, x and x^+ , respectively. Similar to MoCo v2, the weights of the teacher encoder are updated using EMA. However, DINO also removes the dependency on negative samples; in the absence of negative embeddings, this method avoids *model collapse* using a *centering* operation. This operation first computes the centers of the positive embeddings using EMA, $c = \lambda_c c + (1 - \lambda_c) \frac{1}{B} \sum_{i=1}^B x_i^+$, then subtracts the centers c from the

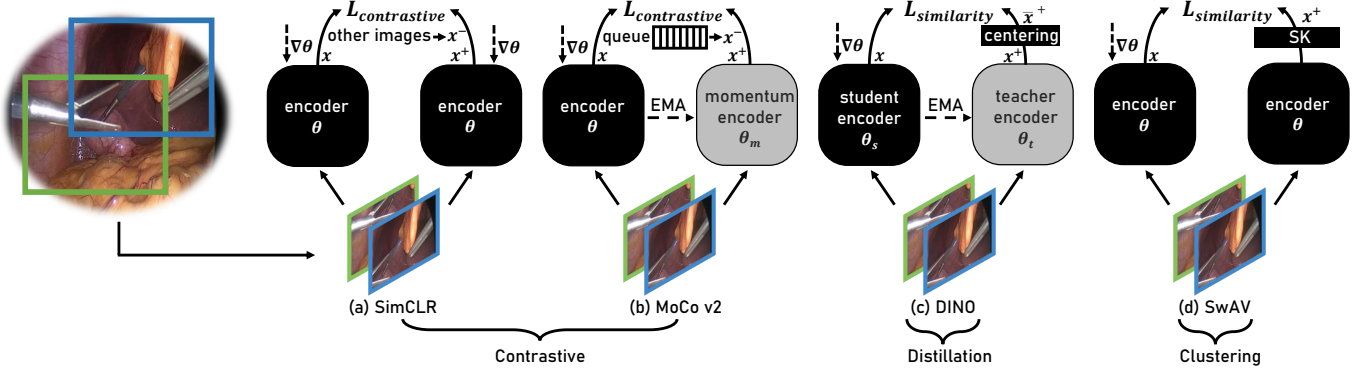


Fig. 4. We study four SSL methods from three categories: contrastive (SimCLR (Chen et al., 2020a) and MoCo v2 (He et al., 2020; Chen et al., 2020b)), distillation-based (DINO (Caron et al., 2021)), and clustering-based (SwAV (Caron et al., 2020)). SimCLR and MoCo v2, as contrastive methods, use embeddings from other images or a queue to generate negative embeddings (x^-), respectively. MoCo v2 and DINO use an explicit momentum encoder whose weights are updated using an exponential moving average (EMA). $\nabla\theta$ are the gradients of the encoder’s weights θ , computed using a contrastive loss ($L_{contrastive}$) for SimCLR and MoCo v2 and a similarity loss ($L_{similarity}$) for DINO and SwAV. DINO uses a centering operation, and SwAV uses a non-differentiable Sinkhorn-Knopp (SK) transform (Cuturi, 2013) to avoid model collapse in the absence of negative embeddings.

positive embeddings to compute the mean-centered positive embeddings, $\bar{x}^+ = x^+ - c$. Here, B is a batch dimension and λ_c is a centering decay parameter. The similarity loss

$$L_{similarity} = - \sum \text{softmax}(x/\tau_s) \log(\text{softmax}(\bar{x}^+/\tau_t)) \quad (2)$$

is computed as a cross-entropy loss between the reference positive embedding, x , and mean-centered positive embeddings, \bar{x}^+ . The $\text{softmax}()$ function normalizes embeddings that are scaled differently using temperature parameters τ_s and τ_t for the student and teacher encoders, respectively.

SwAV (Caron et al., 2020) circumvents the need for negative embeddings by first transforming the positive embedding pair, x and x^+ , to learned prototype embeddings, \bar{x} and \bar{x}^+ and then performing online clustering of the learned prototype embeddings using the Sinkhorn-Knopp (SK) algorithm (Cuturi, 2013). The SwAV similarity loss is

$$L_{similarity} = \mathcal{D}_{KL}(\bar{x} \parallel \text{SK}(\bar{x}^+)), \quad (3)$$

where \mathcal{D}_{KL} is the Kullback-Leibler divergence.

3.3. Hyperparameter study design

In the hyperparameter study (Fig. 1, A), we aim to better understand the sensitivity of each SSL method to hyperparameter variations and establish a set of **recommended** values that will later serve in practical use cases of semi-supervised learning, as part of the data supply study (Fig. 1, B). To this end, we select a subset of 5 critical hyperparameters:

- Type of augmentation
- Batch size
- Epochs
- Sampling rate
- Type of initialization

Table 1. Observed SSL hyperparameters. Defaults are used in the hyperparameter study. Recommended values (best overall performance in the hyperparameter study) are used in the data supply study.

	Defaults	Recommended	
Augmentations	Multi-Crop	8	2
	Color	On	On
	Geometric	On	On
	Strong-color	Off	Off
Batch size	512	256	
Epochs	300	300	
Sampling rate	1	5	
Initialization	Scratch	Imagenet fully supervised	

We then carefully analyze the influence of all 5 on the performance, for the tasks of phase recognition and tool presence detection on the Cholec80 dataset. Each of those 5 hyperparameters defines a group of experiments, where the relevant hyperparameter varies while others are set to the default values shown in Table 1. For each value of that hyperparameter, 4 models are trained - one for each selected SSL method. Linear evaluation is then performed on the validation set, i.e. by training a linear classifier added on top of the frozen backbone layers, for tool and phase tasks separately. This validation protocol, commonly used in SSL (Feichtenhofer et al., 2021a), verifies here how well each method, for that particular hyperparameter value, maps frames to linearly separable vector representations that are consistent in terms of phase and tool content. Details for each experiment group are provided in the following paragraphs.

Augmentations. Data augmentation is a crucial aspect of SSL methods (Chen et al., 2020a): learning persistent feature representations between different *views* of the same image (i.e. between different augmented versions of the original image), is the implicit task that SSL methods leverage in order to produce powerful representations of unlabeled data. Hence, it is imperative to understand the impact of this parameter when shifting to different domains and tasks. While an exhaustive

search of augmentations is beyond the scope of this study², we decided to focus on broad categories of commonly used augmentation techniques to train SSL methods (Caron et al., 2021; Chen et al., 2020a; He et al., 2020), defined here as *Color*, *Geometric*, *Strong-color* and *Multi-Crop*. Fig. 5 provides a description for each category.

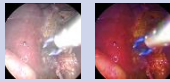
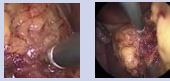
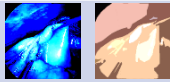
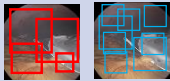
Data augmentation type		Description
Color		Realistic color adjustments <i>brightness, contrast, saturation</i>
		Spatial affine transforms <i>rotation, translation, scaling, shearing</i>
Strong Color		Heavy color corruption <i>inversion, posterization, solarization</i>
		Cropped duplicate views, including 2 at a high resolution <i>2 views, 4 views, 8 views</i>

Fig. 5. Data augmentation types involved in the hyperparameter study

All the mentioned augmentations are randomized during training (Cubuk et al., 2020a); the randomization process follows the implementation of Goyal et al. (2021).

Multi-Crop is set to 2, 4, or 8 crops with 2 crops always sampled at a high resolution following Caron et al. (2020). Each of the other 3 augmentation types is either *on* or *off*. Considering all the possible combinations, we examine a total of $3 * 2^3 = 24$ configurations for augmentations.

Batch size. Batch size is a crucial hyperparameter in SSL methods: SimCLR (Chen et al., 2020a) established a positive correlation between performance and batch size attributed to the size of the pool of negative samples to draw from during training. The other 3 approaches have presented the ability to better function with smaller batches as an advantage, cutting down memory requirements.

To examine these claims, we use batches of sizes 128, 256, 512 and 1024.

Epochs. Previous studies have shown that training time could largely impact SSL performance. Given this, we investigate the impact of training time by training each SSL method for 50, 100, 200 and 300 epochs.

Sampling rate. While the SSL methods we test are designed for still images, we can apply them to video inputs by simply extracting individual frames from each video. A key consideration when doing so is the frame sampling rate, as this can affect the relative homogeneity among various input images. In this aspect, surgical videos pose a particularly interesting technical setting, as they tend to provide a stable context, and the only changes across frames, even for several minutes of video, are manipulations of organs and medical tools in the field of view. Consequently, while increasing the

number of frames sampled per second dramatically increases the available training data, it is unclear whether this additional data would be beneficial for SSL methods.

We experiment with sampling videos at 0.1, 0.33, 0.5, 1, 3, and 5 frames per second (fps).

3.4. Data supply study design

In contrast with the previous section, the data supply study (Fig. 1, B) operates with a completely fixed set of recommended hyperparameters (Table 1), suitable for examining our chosen SSL methods in practical semi-supervision use cases: instead of freezing the backbone after self-supervised training, here we finetune it with phase or tool annotations in conjunction with a linear classifier. For phase recognition, we also observe the performance obtained by adding a temporal model (TCN, Czempiel et al. (2020)) after this step and finetuning it separately as well: this provides a strong point of comparison against the state of the art, while also gauging the representations learned through SSL when used in a temporal context.

Labeled data supply. We first focus on labeled data only. Performance with respect to annotated data availability (Fig. 1, B1) is examined in three settings, with supervised finetuning performed after SSL on 40 videos (100% of the entire Cholec80 training set), 10 videos (25%), or 5 videos (12.5%) of the full data. To mitigate the effect of outliers, experiments for the last two settings are replicated on 3 randomly selected sets of videos. In all these configurations, the same 40 unlabeled videos are used for self-supervised pretraining.

Unlabeled data supply. In addition to this core set of experiments focusing exclusively on varying labeled data, we select one SSL method - MoCo v2 - and examine how it reacts to changes in the amount of unlabeled data (Fig. 1, B2) used for self-supervised training: from 1, to 10, 20, 40, and finally 80 unlabeled videos. Results are reported for varying numbers of labeled videos used for finetuning

4. Results

4.1. Dataset Splits and Evaluation Metrics

In all our experiments, following previous literature (Czempiel et al., 2020; Jin et al., 2018; Twinanda et al., 2016b; Czempiel et al., 2021), we use 40, 8, and 32 videos from Cholec80 as our total available pool of training videos, our validation set, and our test set, respectively.

In the hyperparameter study, we perform SSL pretraining on the entire pool of 40 training videos and report the results on the validation set.

In the data supply study, we further conduct semi-supervised experiments with 5 videos (12.5% of Cholec80 training set) and 10 videos (25% of Cholec80 training set) of annotations, for which we employ two different sampling strategies. For the comparison with external methods (Table 6), we use the predefined dataset split introduced in Shi et al. (2021) as sampling strategy to enable fair comparisons. However, for the remainder of our experiments (see Tables 3,

²Pretraining a ResNet-50 using SSL with a single hyperparameter setting given our experimental design demands approximately 40 GPU hours using 4 NVIDIA V100s on average across considered methods.

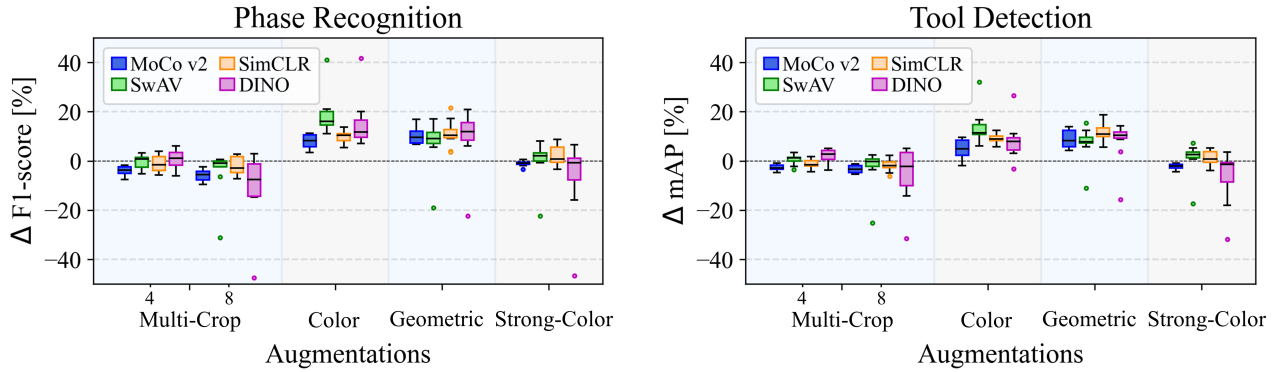


Fig. 6. Performance of each method on Cholec80 varying the augmentation strategy for self-supervised pretraining. For each method and category of augmentations, we show a boxplot with the change in performance from the default no-augmentation setting (using 2 crops for *Multi-Crop*), by enabling that category of augmentation (using 4 or 8 crops for *Multi-Crop*). The boxplot whiskers were set to 1.5 times the interquartile range beyond the first and third quartile; settings outside of this margin were defined as outliers and plotted as dots. Results were obtained using linear evaluation on the validation set. Left: F_1 -score for phase recognition. Right: mAP for tool presence detection.

4, 5, and Figures 12, 13), we either make use of established training splits (Twinanda et al., 2016b) for larger data settings (40, 80 training videos), employ a stratified random sampling approach or random uniform sampling when stratifying is infeasible (1 training video). In each case when randomly sampling, we sample three separate subset splits of the training videos, evaluate model performance on each split, and report the mean and standard deviation across splits. Doing so alleviates selection bias and allows for sound comparisons across methods and experimental settings. Indeed, we find that the variance in performance across dataset splits, particularly in the low-data settings, can surpass performance differences across methods, highlighting the need to sample multiple splits.

For all phase recognition experiments, with the exception of the external comparison (Table 6), we report per-video F1 Score, computed by averaging across each video’s F1 score. In these tables, the standard deviation is presented across the sampled splits. Meanwhile, for the external comparison, we report a *relaxed boundary* per-video F_1 Score, originally introduced in the m2cai16-workflow challenge³ and used by Shi et al. (2021), to enable a fair comparison. The relaxed boundary metric introduces a 10 second ‘relaxed’ period centered around each ground truth phase transition; during these periods, the two consecutive phases are considered to be correct classifications (e.g. phase 4 and phase 5 are both accurate classifications in the 10 seconds before and after the transition from phase 4 to 5). Consequently, the relaxed boundary metric results in higher scores across methods.

For all tool presence detection experiments, we compute mAP across all considered frames and in all the presented tables the standard deviation is calculated across splits.

4.2. Hyperparameter study

We present here the impact of hyperparameters variations on the quality of the representations learned by the SSL

methods we selected, following the setup described in Section 3.3⁴.

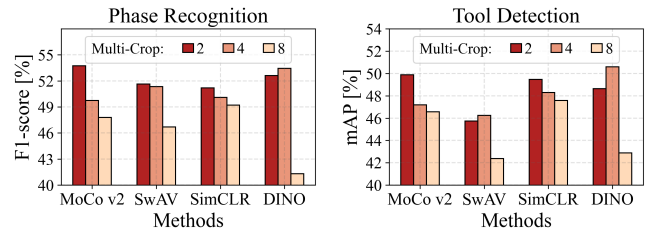


Fig. 7. Performance of each method on Cholec80 varying the Multi-Crop augmentation strategy for self-supervised pretraining: 2,4 or 8 crops (2 high resolution crops, remaining low resolution). Results were obtained using linear evaluation on the validation set. Left: F_1 -score for phase recognition. Right: mAP for tool presence detection.

Augmentations. In order to evaluate the impact of each of the four augmentation categories, we show the improvement introduced by the presence of each category across all the considered experiments for each SSL method. For every augmentation category, we examine the change in performance - ΔF_1 and ΔmAP - caused by toggling it *on* (for *Multi-Crop*, by switching it from 2 to either 4 or 8). To this end, in Fig. 6, we plot the following set of samples for the *Multi-Crop* (4 and 8 crops - **MC4** and **MC8**), *Color* (**C**), *Geometric* (**G**) and

⁴GPU training presents some non-determinism that is not trivial to avoid. Because performing several reruns of every experiment in the hyperparameter study would be computationally impractical, we do so for one method selected at random and present the standard deviation when performing linear evaluation for both downstream tasks in order to contextualize our results. The standard deviation across 5 reruns for this selection for phase recognition and tool presence detection is 0.7 % F1 and 0.7 % mAP, respectively.

³<http://camma.u-strasbg.fr/m2cai2016/index.php/program-challenge/>

Strong-Color (**S**) augmentation experiments, respectively:

$$\begin{aligned}
 \mathbf{MC8} &= \{(mc_8 \ c_i g_j s_k - mc_2 c_i g_j s_k)_{i=\{1,0\},j=\{1,0\},k=\{1,0\}}\}, \\
 \mathbf{MC4} &= \{(mc_4 \ c_i g_j s_k - mc_2 c_i g_j s_k)_{i=\{1,0\},j=\{1,0\},k=\{1,0\}}\}, \\
 \mathbf{C} &= \{(mc_i c_1 g_j s_k - mc_i c_0 g_j s_k)_{i=\{2,4,8\},j=\{1,0\},k=\{1,0\}}\}, \\
 \mathbf{G} &= \{(mc_i c_j g_1 s_k - mc_i c_j g_0 s_k)_{i=\{2,4,8\},j=\{1,0\},k=\{1,0\}}\}, \\
 \mathbf{S} &= \{(mc_i c_j g_k s_1 - mc_i c_j g_k s_0)_{i=\{2,4,8\},j=\{1,0\},k=\{1,0\}}\},
 \end{aligned}
 \tag{4}$$

where *mc* is *Multi-Crop* augmentation and can take the values 2,4,8; *c*, *g*, *s* are, respectively, *Color*, *Geometric* and *Strong-Color* augmentations, which can either be toggled *on* (1) or *off* (0). For each augmentation setting, statistics for ΔF_1 and ΔmAP are collected and represented as boxplots. Average performance for each *Multi-Crop* setting is also shown separately in Fig. 7.

Experimental results for phase recognition and tool presence detection, shown in Fig. 6, demonstrate the clear impact that augmentation strategies have on the quality of the learned representations, consistent across methods and tasks. We make three main observations:

(1) In general, increasing the number of low-resolution views on *Multi-Crop* negatively impacts performance. From 2 crops for MoCo v2, switching to 4 crops cuts down phase recognition F_1 by 3.5%; switching to 8 cuts it down by 4.5%. This represents an important deviation from typical results in the natural image domain, where additional low-resolution views in *Multi-Crop* generally positively correlate with improved performance (Caron et al., 2020, 2021). A possible explanation may be the weaker value of ensuring ‘local-to-global’ feature invariance in the surgical domain; in surgical phase recognition, for example, discriminative cues may be scattered in the entire image, and be significant only if considered as a whole: in light of this, forcing ‘local-to-global’ invariant features may be challenging, or even undesirable in this domain.

(2) The *Color* augmentation consistently and significantly improves performance. This is generally analogous to results on the natural image domain (Feichtenhofer et al., 2021a): as pointed out in (Chen et al., 2020a), augmentations like *Multi-Crop* and *Geometric* mostly preserve the original color distribution, leaving this as an easy shortcut for the network to solve the predictive task; the *Color* augmentation is therefore an important factor in learning meaningful representations.

(3) DINO is the method most affected by the specific choice of augmentation; in particular, representation quality dramatically drops when both *Multi-Crop* and *Strong-Color* augmentations are used; a possible explanation may derive from the general observation on *Multi-Crop* made previously: compared to the other methods, DINO explicitly enforces the ‘local-to-global’ feature invariance, by passing all views to the student, but only global *views* to the teacher. While this task is intrinsically difficult in the surgical domain, for the previously discussed reasons, it may be made even more challenging by the presence of the *Strong-Color* augmentation, leading to unreliable feature representations.

Batch size. Overall, larger batch sizes do not improve feature quality. Clear improvements are only perceivable between 128

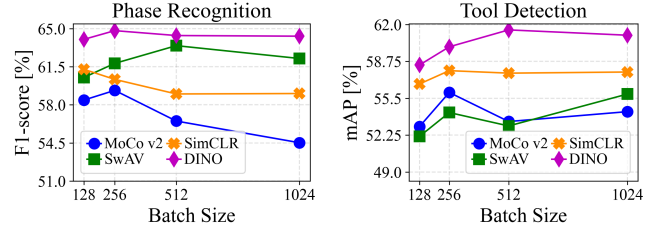


Fig. 8. Performance of each method on Cholec80 varying the batch size used for self-supervised pretraining. Results were obtained using linear evaluation on the validation set. Left: F_1 -score for phase recognition. Right: mAP for tool presence detection.

and 256 (up to 4.8% F_1 for phase recognition, 5.6% mAP for tool detection) across all tasks and methods - except for phase recognition with SimCLR. Results for 256 and above, however, generally contradict claims from other SSL works (Chen et al., 2020a; Caron et al., 2020, 2021), especially on the phase recognition task (Fig. 8): from 256 to 1024, MoCo v2’s F_1 score drops by 5.5%. No clear positive impact of increasing batch size past 256 can be seen on tool presence detection either (Fig. 8).

This inconsistency with results obtained on natural images is possibly due to differences in data scale, since Cholec80 (at 1 fps: $\sim 10^5$ samples, 7 classes) is far smaller than ImageNet ($> 10^6$ samples, 10^3 classes). During training, batches are therefore sampled under completely different conditions; since SSL methods, in the absence of labels, rely heavily on negative and positive samples to separate classes, this can affect the final performance.

In the literature, one documented adverse effect of larger batches in SSL is shown by Chen et al. (2020a) on SimCLR, when the batch size is pushed up to high values (>2048). A scaled back version of this phenomenon might be at play here.

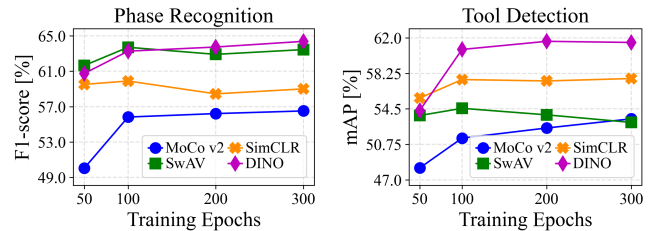


Fig. 9. Performance of each method on Cholec80 varying the number of epochs used for self-supervised pretraining. Results were obtained using linear evaluation on the validation set. Left: F_1 -score for phase recognition. Right: mAP for tool presence detection.

Epochs. Overall, phase recognition and tool presence detection performance (Fig. 9) tends to saturate as epochs increase, with nuances from one SSL method to another. SwAV and SimCLR in particular clearly peak earlier than the other two methods at 100 epochs, losing up to 2% phase recognition F_1 and 2% tool presence detection mAP afterwards. In contrast, MoCo v2 and DINO improve over the entire 300-epoch training period, with, nonetheless, a

noticeable slowdown after 100 epochs.

This disparity could be a result of including a momentum encoder (used by both MoCo v2 and DINO). The momentum encoder enables a greater diversity in pairs of latent vectors generated by the network backbone during training: in MoCo v2, via a greater set of negative samples to choose from, and in DINO, via the teacher network incorporating context from a wider variety of samples. Consequently, longer training may allow models to learn more robust representations.

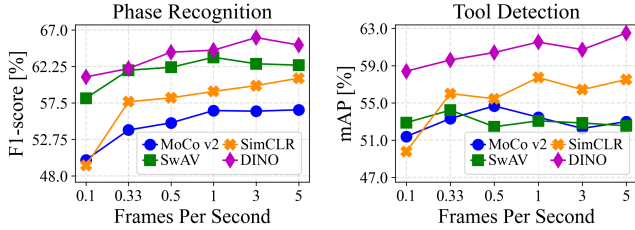


Fig. 10. Performance of each method on Cholec80 varying the Frames Per Second for self-supervised pretraining. Results were obtained using linear evaluation on the validation set. Left: F_1 -score for phase recognition. Right: mAP for tool presence detection.

Sampling rate. As previously stated, surgical videos pose a particularly interesting technical setting for SSL research in general because surgical videos often provide a very stable context while the anatomy in the scene is manipulated. While increasing the number of frames sampled per second could dramatically expand the available training data, performance might not increase due to redundancy. Indeed, with the 5 sampling rates examined here, we observe marginal utility in sampling frames beyond a certain frequency. For both tasks, when sampling frames at over 1 fps, we observe no consistent improvement across methods or tasks when training with higher sampling rates (Fig. 10). This is an important finding that may lend useful intuition to researchers applying SSL to domains with similar motion characteristics on how best to allocate computational resources, when training these intensive methods comes with a sizeable financial and environmental cost. To note, for a fair comparison, we perform this experiment here assuming an equal distribution of computational resources, i.e. we evaluated the models after performing self-supervised pretraining for the same number of iterations for each frame rate. This implies that the 1 fps experiments were trained for ~ 5 times as many epochs as the 5 fps experiments.

Initialization. In general computer vision, the common practice for SSL experimentation is to train models to learn self-supervised representations entirely from scratch (i.e. random weights) before using these representations to attempt to replicate fully supervised performance - for image recognition on Imagenet, as a prominent example. Weights obtained in this manner are then intended to serve as initialization for downstream tasks. However, in surgical computer vision, Imagenet fully supervised weights are considered as a readily available resource: the practice of using them to initialize models is tacitly recognized as standard by the community.

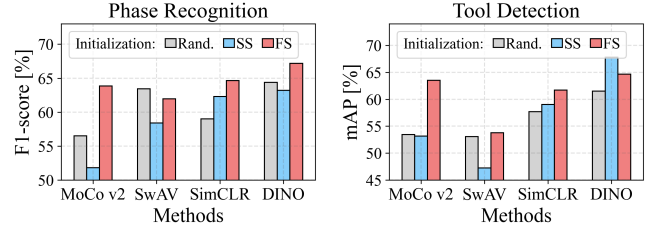


Fig. 11. Performance of each method on Cholec80 varying the network initialization strategies before performing self-supervised pretraining: random initialization (Rand.), ImageNet self-supervised (SS), ImageNet fully-supervised (FS). Results were obtained using linear evaluation on the validation set. Left: F_1 -score for phase recognition. Right: mAP for tool presence detection.

The choice of initialization is therefore not trivial, with 3 options available before starting SSL training on surgical data:

1. “Rand.”: randomly initializing weights
2. “SS”: initializing weights with self-supervised pretraining on ImageNet
3. “FS”: initializing weights with fully supervised pretraining on ImageNet

Across all SSL methods (Fig. 11), models initialized with “FS” significantly outrank models with “Rand.” or “SS.” initialization; most noticeably with MoCo v2 (up to +12% phase recognition F_1 , +11% tool detection mAP compared to the other two). Results between “Rand.” and “SS.” do not clearly favor one over the other. This is obviously a major difference from general computer vision, which expects models initialized from scratch to improve on any downstream task through SSL training. One explanation for this discrepancy could be the set of invariances learned in the natural domain, which may not apply to surgical images.

Hyperparameter study conclusion. This study provides a detailed view of each SSL method’s reaction to changes in parametrization when operating in the surgical domain, exposing noteworthy differences with the natural domain - regarding augmentations, batch size and initialization most prominently. However, when considering all four SSL methods and both tasks simultaneously, global trends can be difficult to clearly point out. To achieve this in a quantitative and principled manner, we define a selection metric, defined as the average of all phase recognition F_1 scores and tool presence detection mAPs across all methods for a given setting. Using this, we are able to rank the values of a given hyperparameter by overall performance across downstream tasks, then retain the best. This forms a global set of **recommended settings** (Table 1) for SSL in the surgical domain.

In Table 2, we present the results ranked according to this selection metric for each ablation to facilitate the analysis of invariant trends for methods and tasks. For each hyperparameter, we summarize the trends in brief below:

- Sampling rate: We observe only a marginal utility of increasing the sampling rate beyond a certain point, with the selection metric saturating past 0.33 fps.

Table 2. The average results across methods are presented for phase recognition, tool presence detection and the average across both tasks (Selection metric). For each individual ablation, results are presented in descending order of performance according to the Selection metric. The Setting column refers to the value of the parameter being ablated, while all other settings are kept to the default values specified in Table 1. For the augmentation ablation, we use the following notations: MC - Multi-Crop, C - Color, G - Geometric, S - Strong-color; for the MC setting columns, we specify total number of crops used (including 2 high-resolution crops) and for the S, G, and C setting columns, we specify whether those augmentation categories were included or “on”.

Ablation	Setting	Selection metric	Phase (F1)	Tool (mAP)	Ablation	Setting				Selection metric	Phase (F1)	Tool (mAP)
						MC	C	G	S			
Sampling rate	5.0	58.8	61.2	56.4	Augmentations	2	✓	✓	✗	60.0	63.5	56.5
	1.0	58.6	60.8	56.4		2	✓	✓	✓	59.6	63.2	55.9
	3.0	58.4	61.2	55.6		4	✓	✓	✓	59.1	61.7	56.5
	0.5	57.8	59.8	55.7		4	✓	✓	✗	58.9	61.1	56.8
	0.33	57.3	58.8	55.8		8	✓	✓	✗	58.6	60.8	56.4
	0.1	53.9	54.6	53.1		8	✓	✓	✓	54.7	56.4	53.1
Batch size	256	59.3	61.6	57.1		2	✗	✓	✗	53.7	55.4	52.0
	1024	58.6	60.0	57.3		2	✗	✓	✓	53.3	54.6	51.9
	512	58.6	60.8	56.4		...						
	128	58.1	61.1	55.1		8	✓	✗	✓	45.5	47.5	43.6
Initialization	FS	62.7	64.4	60.9		4	✗	✗	✓	41.2	42.2	40.2
	Rand	58.6	60.8	56.4		2	✗	✗	✓	40.2	41.1	39.4
	SS	57.9	58.9	56.8	8	✗	✗	✓	37.3	37.8	36.8	
Epochs	300	58.6	60.8	56.4	4	✗	✗	✗	37.3	36.9	37.6	
	100	58.4	60.7	56.1	2	✗	✗	✗	37.0	37.2	36.8	
	200	58.3	60.3	56.4	8	✗	✗	✗	36.8	35.8	37.7	
	50	55.5	58.0	53.0	8	✗	✓	✓	33.1	31.4	34.8	

- **Batch size:** The results show that for the considered tasks and dataset, SSL method performance is mostly robust to variations of batch size. Varying the batch size between 128-1024 results in a maximum variation of 1.1% F1 and 2% mAP on average across methods for phase recognition and tool presence detection, respectively.
- **Initialization:** Initialization before self-supervised representation learning proves to be a critical hyperparameter with significant and consistent gains in performance across both methods and tasks. Initializing with Imagenet fully supervised (“FS”) weights proves to be the optimal setting amongst the considered initializations.
- **Epochs:** For both considered tasks, we see significant gains in performance up to 100 epochs after which it plateaus, with an average variation of 0.4% F1 and 0.4% mAP between 100 and 300 epochs.
- **Augmentations:** Interestingly, we observe largely consistent trends for different augmentation settings for both tasks. Color and geometric augmentations feature consistently in top performing augmentation settings. On average across methods, the addition of multiple low-resolution views and strong color augmentations has a less clear impact on performance.

4.3. Data supply study

The recommended choice of hyperparameters mentioned above provides, on average, close to optimal conditions for observing our panel of SSL methods in practical use cases, with varying quantities of labeled or unlabeled data. Our proposed usage of SSL is defined as follows: self-supervised

training is performed in the surgical domain before finetuning for surgical downstream tasks.

Labeled data supply. In this section of the data supply study, self-supervised training is first performed on the entire training set of Cholec80 with the recommended hyperparameters. Surgical downstream task finetuning is then applied using variable amounts of labeled data: 40 videos (100% of the training set), or in semi-supervision with 10 videos (25%) or 5 videos (12.5%); for these last two settings the portions of the training set are drawn following a stratified random sampling approach (see Sec. 4.1). Results for these experiments are reported in Tables 3 (phase recognition on single frames), 4 (phase recognition on videos with a temporal model), and 5 (tool presence detection). We compare our proposed usage of SSL (“ours”) on Cholec80 using the recommended hyperparameters (Table 1) with the mode of operation borrowed from general computer vision (“base”) - i.e. finetuning directly from weights pretrained with SSL on Imagenet. The bottom row in each table (“No SSL”) provides an additional point of comparison, where we finetune models initialized with fully supervised Imagenet weights without any SSL.

In low-label settings (10, 5 videos), adding any of the 4 SSL methods systematically improves the performance on both surgical tasks, compared to direct finetuning from supervised Imagenet weights without SSL. This improvement reaches up to 5.7% for single-frame phase recognition, 4.8% for temporal phase recognition, and 14.7% for tool presence detection. Gains are consistently observed, especially in low-label settings where standard deviation across splits mostly stays underneath 3%. 100% label availability tends to saturate performance on downstream tasks, leaving little room for improvement from SSL; still, results are on par with those

Table 3. Effect of our proposed SSL pretraining in the surgical domain (“Ours”) on surgical phase recognition performance from single frames. “Base” refers to self-supervised pretraining on Imagenet only. “No SSL” refers to fully supervised pretraining on Imagenet only. Bold indicates the best performance for a given number of labeled videos.

Surgical phase recognition F_1 - single frame						
Labels	40 videos		10 videos		5 videos	
	Base	Ours	Base	Ours	Base	Ours
DINO	67.0	66.8	57.0 ± 0.3	58.7 ± 0.4	49.0 ± 5.0	53.1 ± 3.6
MoCo v2	66.1	67.0	55.6 ± 1.4	60.7 ± 1.0	48.6 ± 2.9	54.8 ± 3.9
SimCLR	65.9	67.4	55.6 ± 0.7	60.0 ± 0.7	48.0 ± 3.4	53.9 ± 3.8
SwAV	67.2	66.1	57.1 ± 0.4	58.8 ± 1.4	48.5 ± 3.8	53.9 ± 2.7
No SSL	66.1		55.2 ± 0.4		49.1 ± 3.4	

Table 4. Effect of our proposed SSL pretraining in the surgical domain (“Ours”) on surgical phase recognition performance from videos when finetuning a temporal model (TCN - Czempiel et al. (2020)) on top of the backbones described in Table 3. Bold indicates the best performance for a given amount of labeled videos.

Surgical phase recognition F_1 - temporal						
Labels	40 videos		10 videos		5 videos	
	Base	Ours	Base	Ours	Base	Ours
DINO	78.4	78.9	68.0 ± 0.2	68.3 ± 0.4	61.3 ± 5.9	63.3 ± 3.8
MoCo v2	76.8	77.1	66.6 ± 2.1	71.8 ± 0.6	62.2 ± 3.1	64.3 ± 3.2
SimCLR	76.6	78.6	66.8 ± 0.4	70.3 ± 0.2	59.6 ± 5.0	64.5 ± 2.0
SwAV	78.7	76.9	69.0 ± 0.8	69.3 ± 0.7	59.7 ± 6.7	66.7 ± 0.9
No SSL	77.3		67.0 ± 1.4		62.3 ± 3.3	

Table 5. Effect of our proposed SSL pretraining in the surgical domain (“Ours”) on surgical tool presence detection performance. Bold indicates the best performance for a given amount of labeled videos.

Surgical tool presence detection mAP						
Labels	40 videos		10 videos		5 videos	
	Base	Ours	Base	Ours	Base	Ours
DINO	92.1	93.2	70.1 ± 2.7	81.2 ± 1.4	50.6 ± 1.6	68.7 ± 2.3
MoCo v2	92.9	93.5	70.4 ± 1.3	85.7 ± 1.1	56.5 ± 3.3	74.7 ± 1.8
SimCLR	90.4	93.1	66.7 ± 0.1	83.0 ± 0.9	49.3 ± 1.4	69.7 ± 3.0
SwAV	92.5	92.8	70.5 ± 1.5	79.1 ± 1.7	52.5 ± 1.8	63.0 ± 0.7
No SSL	93.6		77.9 ± 0.8		60.0 ± 2.3	

obtained without SSL for tool presence detection (< 1% difference) and superior for phase recognition for all methods except SwAV, which is equal or very slightly below. Out of the four SSL methods presented here, MoCo v2 performs the best in most situations; for tool presence detection with 5 labeled videos in particular, it surpasses the other three by 5% mAP at least.

Most importantly, these results challenge the generalizability of general computer vision SSL. As demonstrated in Oord et al. (2018); He et al. (2020); Chen et al. (2020b); Caron et al. (2021), self-supervised pretraining on natural images enhances downstream task performance in the natural image domain; however these gains may not carry over to more complex and more specific domains. Indeed, when trained on Imagenet, none of the SSL methods featured here improve performance on surgical downstream tasks compared to the “No SSL” baseline. For phase recognition, this usage of SSL even causes F_1 score to drop by roughly 1%, while for tool presence detection, the degradation reaches up to 8% mAP. Overall, our proposed use of SSL outperforms the “base” usage by up to 6.2% on single-frame phase recognition, 7%

on temporal phase recognition, and 20.4% on tool presence detection.

Finally, we add an external comparison in Table 6 with preexisting semi-supervised studies in surgical computer vision, based on results presented by Shi et al. (2021) for semi-supervised phase recognition on Cholec80, and using the same split and metric definition. As expected, selected SSL methods applied to single-frame models are outranked by other approaches, by up to 12%; however the external methods we compare against use temporal modeling, which gives them a strong advantage. For a fairer comparison, we examine models trained with our selected SSL methods used in conjunction with a temporal model (TCN): in these situations, they surpass preexisting semi-supervised approaches by a substantial amount - up to 14.6%. Top F_1 scores are achieved by DINO (91.8% with all labels), SimCLR (85.4%, 1/4 of labels) and MoCo v2 (81.9%, 1/8 of labels). To note, the architecture we use is fairly simple (CNN - TCN) compared to the more refined designs featured in the external methods; therefore our performance gains derive from the SSL methodology itself, and could further increase with more

Table 6. External comparison with Shi et al. (2021) for semi-supervised surgical phase recognition. Bold indicates the best performance for a given amount of labeled videos used for finetuning.

External comparison - surgical phase recognition F_1					
Labels			40 videos	10 videos	5 videos
External <i>quoted from Shi et al. (2021)</i>	NL-RCNet		82.1	-	-
	NL-RCNet+		84.4	73.95	67.3
	CNN-BiLSTM-CRF		-	75.3	70.9
	MT		-	77.3	71.0
	SurgSSL		-	80.6	78.6
Selected SSL methods <i>metric and split from Shi et al. (2021)</i>	DINO	single frame	78.1	65.3	66.4
		temporal	91.8	81.7	77.7
	MoCo v2	single frame	81.8	73.5	69.6
		temporal	91.0	82.9	81.9
	SimCLR	single frame	84.1	72.8	67.6
		temporal	93.2	85.4	80.3
	SwAV	single frame	85.6	68.4	69.9
		temporal	90.3	80.4	81.5
Baselines <i>metric and split from Shi et al. (2021)</i>	No SSL	single frame	76.8	67.5	57.9
		temporal	90.3	81.6	73.3

advanced architectures. These observations strongly confirm the high value of bringing SSL innovations from general computer vision to the surgical domain.

Unlabeled data supply. Our main experiments examined the performance of SSL in the surgical domain with a fixed quantity of unlabeled data for self-supervised pretraining; in this complementary set of experiments, we observe how SSL reacts when the quantity of unlabeled videos varies. This part of the study is conducted with MoCo v2 exclusively. Overall, our results (Fig. 12 and 13) confirm a valuable benefit of SSL: for the most part, expanding unlabelled data - which is far easier than generating additional annotations - leads to increased performance in downstream surgical tasks. Particularly when few labeled instances are available, we see extremely pronounced improvements brought about by introducing SSL. For example, when only 5 labeled videos are available, self-supervised pretraining on just 10 unlabeled videos adds 5% F_1 for phase recognition and 14% mAP for tool presence detection. These results further reinforce the practicality of utilizing these SSL methods in surgical applications, where working with small datasets is often the norm rather than the exception. We observe, however, two main limitations.

The first is a *saturation* phenomenon, apparent after 10 unlabeled videos; while going from 1 unlabeled video to 10 clearly improves feature quality (phase recognition, finetuning on 10 labeled: +5% F_1 ; tool presence detection, finetuning on 5 labeled: +14% mAP), results for 10 and up carry more ambiguity, with large differences depending on the task. While phase recognition performance slows down but still increases by a noticeable amount (e.g. finetuning on 10 labeled, +3% F_1 from 10 to 80), tool presence detection completely halts.

The second is *dilution* by labeled data: using larger amounts of annotated videos for finetuning pushes downstream performance closer to its limits, which tends to equalize the

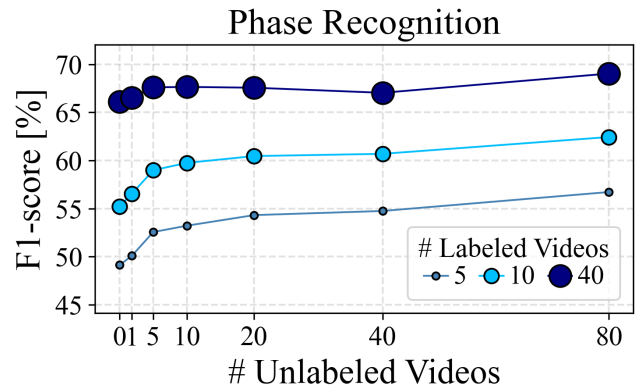


Fig. 12. Single-frame phase recognition performance of MoCo v2 w.r.t. number of unlabeled videos used for self-supervised pretraining, with finetuning on 1 to 40 labeled videos.

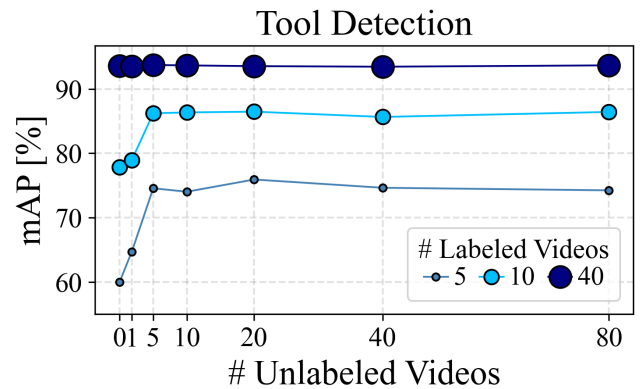


Fig. 13. Tool presence detection performance of MoCo v2 w.r.t. number of unlabeled videos used for self-supervised pretraining, with finetuning on 1 to 40 labeled videos.

effect of adding unannotated videos. For example, for phase recognition from 1 to 80 unlabeled videos, F_1 score increases by 7% with 5 labeled, but only by 4% with 40 labeled. Dilution is much stronger for tool presence detection: from 1 to 80 unlabeled, the total mAP increase with 5 labeled is 14%, while no gain is perceivable at all with 40 labeled.

As evidenced by these observations, the performance growth brought by SSL can slow down as the unlabeled data supply increases, depending on the amount of annotated data available as well as the nature of the task. Tool labels are tied to distinct pieces of visual evidence in the image; their influence on the model's final performance is therefore extremely high, compared to unlabeled videos used in self-supervision. In contrast, phase labels tend to accompany more ambiguous visual cues, which would explain why the advantage of using SSL is much more apparent for surgical phase recognition: a model pretrained with 80 unlabeled videos and finetuned on only 5 labeled videos reaches 57% F_1 , which is the exact same as a model pretrained with 1 unlabeled but finetuned on 10 labeled. Saturation for phase recognition is also much softer than for tool presence detection, suggesting performance can increase even further with more than 80 videos.

5. Conclusion

Despite major progress in the field of self-supervised representation learning over the last several years, its adoption into label-scarce fields like surgery, where it could perhaps have the most significant impact, has been slow. This could be due to the demonstrably heavy reliance on hyperparameter choices that SSL methods demand. In this paper, we conduct an extensive benchmark study to methodically identify effective hyperparameter settings for the task of surgical phase recognition and tool presence detection on the Cholec80 dataset. In doing so, we believe this work could serve as a strong basis for the application of SSL in surgery and lend intuition on how best to extend this work beyond the studied tasks and datasets.

Requiring over 7000 GPU hours, the hyperparameter study demonstrates that this exploration is pivotal to the practical utility of SSL in settings such as semi-supervised learning. For example, initializing the base architecture using Imagenet weights before SSL pretraining critically provided consistent, marked boosts in performance over all other initializations. While random initialization before performing self-supervised representation learning is the standard practice in other large studies, perhaps because of the relative size of the considered datasets, this example highlights the need for principled, adaptable methods to identify optimal settings for other domains. Additionally, domain characteristics could indicate the most significant parameters to prioritize for searches. For instance, in our experiments, relatively slow motion patterns may explain why sampling frames at higher rates for representation learning provides little to no improvement beyond a certain point.

In the data supply study, SSL pretraining shows promising boosts in performance for all methods, particularly in label-scarce scenarios for both phase recognition and tool presence

detection. Interestingly, these methods even outperform state-of-the-art methods for semi-supervised phase recognition using only generic representational features. These results are strongly indicative of the value of targeting surgical applications using these SSL methods, which, within certain limits, can be enhanced by simply incorporating additional unannotated data.

Future work could look beyond the considered datasets and tasks. The generalizability of these features across surgical centers or their integration with decentralized learning techniques such as federated learning (McMahan et al., 2017) may enable research into more robust model designs for surgical applications (Kassem et al., 2022) and eventually real-world deployment. Further, studies on the generalizability of representations learned across surgical procedures may significantly boost the utility of the few, precious datasets that are publicly available for surgical data science research. Another natural progression from this work is to apply these findings to recent work in spatio-temporal representation learning and adapt them to the unique characteristics of surgical videos.

Finally, we note that only a select subset of trends were presented for analysis in this work presenting results aggregated across methods, splits or other experimental settings. With around 500 experiments run over 9000 GPU hours, we will disclose complete results for the experiments conducted in this work, in order to facilitate future research on SSL in surgery. The code will be made available at <https://github.com/CAMMA-public/SelfSupSurg>.

Acknowledgements This work was partially supported by French state funds managed by the ANR under references ANR-20-CHIA-0029-01 (National AI Chair AI4ORSafety), ANR-10-IAHU-02 (IHU Strasbourg) and ANR-16-CE33-0009 (DeepSurg). It was partially supported by funding from the European Union's Horizon 2020 research and innovation program under the Marie Skłodowska-Curie grant agreement No 813782 (ATLAS) and by a PhD fellowship from Intuitive Surgical. It was granted access to the HPC resources of IDRIS under the allocations 2021-AD011011638R1, 2021-AD011012715, 2021-AD011012832, 2021-AD011011507R1, and 2021-AD011011640R1.

References

- Ahsan, U., Madhok, R., Essa, I.A., 2019. Video jigsaw: Unsupervised learning of spatiotemporal context for video action recognition, in: IEEE Winter Conference on Applications of Computer Vision, WACV 2019, IEEE. pp. 179–189. URL: <https://doi.org/10.1109/WACV.2019.00025>, doi:10.1109/WACV.2019.00025.
- Al Hajj, H., Lamard, M., Conze, P.H., Cochener, B., Quellec, G., 2018. Monitoring tool usage in surgery videos using boosted convolutional and recurrent neural networks. *Medical image analysis* 47, 203–218.
- Asano, Y.M., Rupprecht, C., Vedaldi, A., 2019. Self-labelling via simultaneous clustering and representation learning. arXiv preprint arXiv:1911.05371.

- Bachman, P., Hjelm, R.D., Buchwalter, W., 2019. Learning representations by maximizing mutual information across views. arXiv preprint arXiv:1906.00910 .
- Benaïm, S., Ephrat, A., Lang, O., Mosseri, I., Freeman, W.T., Rubinstein, M., Irani, M., Dekel, T., 2020. Speednet: Learning the speediness in videos, in: 2020 IEEE/CVF Conference on Computer Vision and Pattern Recognition, CVPR 2020, Seattle, WA, USA, June 13-19, 2020, Computer Vision Foundation / IEEE. pp. 9919–9928. doi:10.1109/CVPR42600.2020.00994.
- Blum, T., Feußner, H., Navab, N., 2010. Modeling and segmentation of surgical workflow from laparoscopic video, in: Jiang, T., Navab, N., Pluim, J.P.W., Viergever, M.A. (Eds.), Medical Image Computing and Computer-Assisted Intervention - MICCAI 2010, 13th International Conference, Beijing, China, September 20-24, 2010, Proceedings, Part III, Springer. pp. 400–407. URL: https://doi.org/10.1007/978-3-642-15711-0_50, doi:10.1007/978-3-642-15711-0_50.
- Bodenstedt, S., Wagner, M., Katic, D., Mietkowski, P., Mayer, B., Kenngott, H., Müller-Stich, B., Dillmann, R., Speidel, S., 2017. Unsupervised temporal context learning using convolutional neural networks for laparoscopic workflow analysis. arXiv .
- Caron, M., Bojanowski, P., Joulin, A., Douze, M., 2018. Deep clustering for unsupervised learning of visual features, in: Proceedings of the European Conference on Computer Vision (ECCV), pp. 132–149.
- Caron, M., Misra, I., Mairal, J., Goyal, P., Bojanowski, P., Joulin, A., 2020. Unsupervised learning of visual features by contrasting cluster assignments. arXiv preprint arXiv:2006.09882 .
- Caron, M., Touvron, H., Misra, I., Jégou, H., Mairal, J., Bojanowski, P., Joulin, A., 2021. Emerging properties in self-supervised vision transformers. arXiv preprint arXiv:2104.14294 .
- Carreira, J., Zisserman, A., 2017. Quo vadis, action recognition? A new model and the kinetics dataset, in: 2017 IEEE Conference on Computer Vision and Pattern Recognition, CVPR 2017, Honolulu, HI, USA, July 21-26, 2017, IEEE Computer Society. pp. 4724–4733. URL: <https://doi.org/10.1109/CVPR.2017.502>, doi:10.1109/CVPR.2017.502.
- Chen, T., Kornblith, S., Norouzi, M., Hinton, G., 2020a. A simple framework for contrastive learning of visual representations, in: International conference on machine learning, PMLR. pp. 1597–1607.
- Chen, X., Fan, H., Girshick, R., He, K., 2020b. Improved baselines with momentum contrastive learning. arXiv preprint arXiv:2003.04297 .
- da Costa Rocha, C., Padoy, N., Rosa, B., 2019. Self-supervised surgical tool segmentation using kinematic information, in: 2019 International Conference on Robotics and Automation (ICRA), IEEE. pp. 8720–8726.
- Cubuk, E.D., Zoph, B., Shlens, J., Le, Q., 2020a. Randaugment: Practical automated data augmentation with a reduced search space, in: Larochelle, H., Ranzato, M., Hadsell, R., Balcan, M., Lin, H. (Eds.), Advances in Neural Information Processing Systems 33: Annual Conference on Neural Information Processing Systems 2020, NeurIPS 2020, December 6-12, 2020, virtual. URL: <https://proceedings.neurips.cc/paper/2020/hash/d85b63ef0ccb114d0a3bb7b7d808028f-Abstract.html>.
- Cubuk, E.D., Zoph, B., Shlens, J., Le, Q.V., 2020b. Randaugment: Practical automated data augmentation with a reduced search space, in: Proceedings of the IEEE/CVF Conference on Computer Vision and Pattern Recognition Workshops, pp. 702–703.
- Cuturi, M., 2013. Sinkhorn distances: Lightspeed computation of optimal transport, in: Burges, C.J.C., Bottou, L., Ghahramani, Z., Weinberger, K.Q. (Eds.), Advances in Neural Information Processing Systems 26: 27th Annual Conference on Neural Information Processing Systems 2013. Proceedings of a meeting held December 5-8, 2013, Lake Tahoe, Nevada, United States, pp. 2292–2300. URL: <https://proceedings.neurips.cc/paper/2013/hash/af21d0c97db2e27e13572cbf59eb343d-Abstract.html>.
- Czempiel, T., Paschali, M., Keicher, M., Simson, W., Feussner, H., Kim, S.T., Navab, N., 2020. TeNCO: Surgical phase recognition with multi-stage temporal convolutional networks, in: MICCAI.
- Czempiel, T., Paschali, M., Ostler, D., Kim, S.T., Busam, B., Navab, N., 2021. Opera: Attention-regularized transformers for surgical phase recognition, in: de Bruijne, M., Cattin, P.C., Cotin, S., Padoy, N., Speidel, S., Zheng, Y., Essert, C. (Eds.), Medical Image Computing and Computer Assisted Intervention - MICCAI 2021 - 24th International Conference, Strasbourg, France, September 27 - October 1, 2021, Proceedings, Part IV, Springer. pp. 604–614. URL: https://doi.org/10.1007/978-3-030-87202-1_58, doi:10.1007/978-3-030-87202-1_58.
- Deng, J., Dong, W., Socher, R., Li, L.J., Li, K., Fei-Fei, L., 2009. Imagenet: A large-scale hierarchical image database, in: 2009 IEEE conference on computer vision and pattern recognition, Ieee. pp. 248–255.
- Dergachyova, O., Bouget, D., Hualmé, A., Morandi, X., Jannin, P., 2016. Automatic data-driven real-time segmentation and recognition of surgical workflow. Int. J. Comput. Assist. Radiol. Surg. 11, 1081–1089. URL: <https://doi.org/10.1007/s11548-016-1371-x>, doi:10.1007/s11548-016-1371-x.
- Diba, A., Sharma, V., Gool, L.V., Stiefelwagen, R., 2019. Dynamonet: Dynamic action and motion network, in: 2019 IEEE/CVF International Conference on Computer Vision, ICCV 2019, Seoul, Korea (South), October 27 - November 2, 2019, IEEE. pp. 6191–6200. URL: <https://doi.org/10.1109/ICCV.2019.00629>, doi:10.1109/ICCV.2019.00629.
- Doersch, C., Gupta, A., Efros, A.A., 2015. Unsupervised visual representation learning by context prediction, in: Proceedings of the IEEE international conference on computer vision, pp. 1422–1430.
- Dosovitskiy, A., Springenberg, J.T., Riedmiller, M., Brox, T., 2014a. Discriminative unsupervised feature learning with convolutional neural networks. Advances in neural information processing systems 27, 766–774.
- Dosovitskiy, A., Springenberg, J.T., Riedmiller, M., Brox, T., 2014b. Discriminative unsupervised feature learning with convolutional neural networks, in: Proceedings of the 27th International Conference on Neural Information Processing Systems - Volume 1, MIT Press, Cambridge, MA, USA. p. 766–774.
- Eigen, D., Fergus, R., 2015. Predicting depth, surface normals and semantic labels with a common multi-scale convolutional architecture, in: 2015 IEEE International Conference on Computer Vision (ICCV), pp. 2650–2658. doi:10.1109/ICCV.2015.304.
- Feichtenhofer, C., Fan, H., Xiong, B., Girshick, R., He, K., 2021a. A large-scale study on unsupervised spatiotemporal representation learning, in: Proceedings of the IEEE/CVF Conference on Computer Vision and Pattern Recognition, pp. 3299–3309.
- Feichtenhofer, C., Fan, H., Xiong, B., Girshick, R.B., He, K., 2021b. A large-scale study on unsupervised spatiotemporal representation learning, in: IEEE Conference on Computer Vision and Pattern Recognition, CVPR 2021, virtual, June 19-25, 2021, Computer Vision Foundation / IEEE. pp. 3299–3309. URL: https://openaccess.thecvf.com/content/CVPR2021/html/Feichtenhofer_A_Large-Scale_Study_on_Unsupervised_Spatiotemporal_Representation_Learning_CVPR_2021_paper.html.
- Fernando, B., Bilén, H., Gavves, E., Gould, S., 2017. Self-supervised video representation learning with odd-one-out networks, in: 2017 IEEE Conference on Computer Vision and Pattern Recognition, CVPR 2017, Honolulu, HI, USA, July 21-26, 2017, IEEE Computer Society. pp. 5729–5738. URL: <https://doi.org/10.1109/CVPR.2017.607>, doi:10.1109/CVPR.2017.607.
- Funke, I., Jenke, A., Mees, S.T., Weitz, J., Speidel, S., Bodenstedt, S., 2018. Temporal coherence-based self-supervised learning for laparoscopic workflow analysis, in: OR 2.0 context-aware operating theaters, computer assisted robotic endoscopy, clinical image-based procedures, and skin image analysis. Springer, pp. 85–93.
- Garrow, C.R., Kowalewski, K.F., Li, L., Wagner, M., Schmidt, M.W., Engelhardt, S., Hashimoto, D.A., Kenngott, H.G., Bodenstedt, S., Speidel, S., Müller-Stich, B.P., Nickel, F., 2021. Machine learning for surgical phase recognition: A systematic review. Annals of Surgery 273. doi:10.1097/SLA.0000000000004425.
- Gidaris, S., Singh, P., Komodakis, N., 2018. Unsupervised representation learning by predicting image rotations. arXiv preprint arXiv:1803.07728 .
- Goyal, P., Caron, M., Lefaudeaux, B., Xu, M., Wang, P., Pai, V., Singh, M., Liptchinsky, V., Misra, I., Joulin, A., et al., 2021. Self-supervised pretraining of visual features in the wild. arXiv preprint arXiv:2103.01988 .
- Grill, J., Strub, F., Altché, F., Tallec, C., Richemond, P.H., Buchatskaya, E., Doersch, C., Pires, B.Á., Guo, Z., Azar, M.G., Piot, B., Kavukcuoglu, K., Munos, R., Valko, M., 2020a. Bootstrap your own latent - A new approach to self-supervised learning, in: Larochelle, H., Ranzato, M., Hadsell, R., Balcan, M., Lin, H. (Eds.), Advances in Neural Information Processing Systems 33: Annual Conference on Neural Information Processing Systems 2020, NeurIPS 2020, December 6-12, 2020, virtual. URL: <https://proceedings.neurips.cc/paper/2020/hash/f3ada80d5c4ee70142b17b8192b2958e-Abstract.html>.
- Grill, J., Strub, F., Altché, F., Tallec, C., Richemond, P.H., Buchatskaya, E.,

- Doersch, C., Pires, B.Á., Guo, Z.D., Azar, M.G., Piot, B., Kavukcuoglu, K., Munos, R., Valko, M., 2020b. Bootstrap your own latent: A new approach to self-supervised learning. *CoRR abs/2006.07733*. URL: <https://arxiv.org/abs/2006.07733>, [arXiv:2006.07733](https://arxiv.org/abs/2006.07733).
- Hadsell, R., Chopra, S., LeCun, Y., 2006. Dimensionality reduction by learning an invariant mapping, in: 2006 IEEE Computer Society Conference on Computer Vision and Pattern Recognition (CVPR'06), IEEE. pp. 1735–1742.
- Han, T., Xie, W., Zisserman, A., 2020. Self-supervised co-training for video representation learning, in: Larochelle, H., Ranzato, M., Hadsell, R., Balcan, M., Lin, H. (Eds.), *Advances in Neural Information Processing Systems 33: Annual Conference on Neural Information Processing Systems 2020, NeurIPS 2020, December 6-12, 2020, virtual*. URL: <https://proceedings.neurips.cc/paper/2020/hash/3def184ad8f4755ff269862ea77393dd-Abstract.html>.
- He, K., Fan, H., Wu, Y., Xie, S., Girshick, R., 2020. Momentum contrast for unsupervised visual representation learning. [arXiv:1911.05722](https://arxiv.org/abs/1911.05722).
- He, K., Zhang, X., Ren, S., Sun, J., 2016. Deep residual learning for image recognition, in: *CVPR*.
- Henaff, O., 2020. Data-efficient image recognition with contrastive predictive coding, in: *International Conference on Machine Learning*, PMLR. pp. 4182–4192.
- Hinton, G., Vinyals, O., Dean, J., et al., 2015. Distilling the knowledge in a neural network. *arXiv preprint arXiv:1503.02531*.
- Hjelm, R.D., Fedorov, A., Lavoie-Marchildon, S., Grewal, K., Bachman, P., Trischler, A., Bengio, Y., 2018. Learning deep representations by mutual information estimation and maximization. *arXiv preprint arXiv:1808.06670*.
- Jenni, S., Meishvili, G., Favaro, P., 2020. Video representation learning by recognizing temporal transformations, in: Vedaldi, A., Bischof, H., Brox, T., Frahm, J. (Eds.), *Computer Vision - ECCV 2020 - 16th European Conference, Glasgow, UK, August 23-28, 2020, Proceedings, Part XXVIII*, Springer. pp. 425–442. URL: https://doi.org/10.1007/978-3-030-58604-1_26, doi:10.1007/978-3-030-58604-1_26.
- Jin, Y., Dou, Q., Chen, H., Yu, L., Qin, J., Fu, C., Heng, P., 2018. Sv-rnet: Workflow recognition from surgical videos using recurrent convolutional network. *IEEE Trans. Medical Imaging* 37, 1114–1126. URL: <https://doi.org/10.1109/TMI.2017.2787657>.
- Jin, Y., Li, H., Dou, Q., Chen, H., Qin, J., Fu, C., Heng, P., 2020. Multi-task recurrent convolutional network with correlation loss for surgical video analysis. *Medical Image Anal.* 59. URL: <https://doi.org/10.1016/j.media.2019.101572>.
- Jing, L., Tian, Y., 2020. Self-supervised visual feature learning with deep neural networks: A survey. *IEEE transactions on pattern analysis and machine intelligence*.
- Jing, L., Tian, Y., 2021. Self-supervised visual feature learning with deep neural networks: A survey. *IEEE Trans. Pattern Anal. Mach. Intell.* 43, 4037–4058. URL: <https://doi.org/10.1109/TPAMI.2020.2992393>, doi:10.1109/TPAMI.2020.2992393.
- Kassem, H., Alapatt, D., Mascagni, P., Consortium, A., Karargyris, A., Padoy, N., 2022. Federated cycling (fedcy): Semi-supervised federated learning of surgical phases. *arXiv preprint arXiv:2203.07345*.
- Kim, D., Cho, D., Kweon, I.S., 2019. Self-supervised video representation learning with space-time cubic puzzles, in: *AAAI 2019, AAAI Press*. pp. 8545–8552. URL: <https://doi.org/10.1609/aaai.v33i01.33018545>, doi:10.1609/aaai.v33i01.33018545.
- Kim, D., Cho, D., Yoo, D., Kweon, I.S., 2018. Learning image representations by completing damaged jigsaw puzzles, in: 2018 IEEE Winter Conference on Applications of Computer Vision (WACV), IEEE. pp. 793–802.
- Kingma, D.P., Ba, J., 2014. Adam: A method for stochastic optimization. *arXiv preprint arXiv:1412.6980*.
- Kuehne, H., Jhuang, H., Garrote, E., Poggio, T.A., Serre, T., 2011. HMDB: A large video database for human motion recognition, in: Metaxas, D.N., Quan, L., Sanfeliu, A., Gool, L.V. (Eds.), *IEEE International Conference on Computer Vision, ICCV 2011, Barcelona, Spain, November 6-13, 2011*, IEEE Computer Society. pp. 2556–2563. URL: <https://doi.org/10.1109/ICCV.2011.6126543>, doi:10.1109/ICCV.2011.6126543.
- Lee, H., Huang, J., Singh, M., Yang, M., 2017. Unsupervised representation learning by sorting sequences, in: *IEEE International Conference on Computer Vision, ICCV 2017, Venice, Italy, October 22-29, 2017*, IEEE Computer Society. pp. 667–676. URL: <https://doi.org/10.1109/ICCV.2017.79>, doi:10.1109/ICCV.2017.79.
- Maier-Hein, L., Eisenmann, M., Sarikaya, D., März, K., Collins, T., Malpani, A., Fallert, J., Feussner, H., Giannarou, S., Mascagni, P., Nakawala, H., Park, A., Pugh, C.M., Stoyanov, D., Vedula, S.S., Cleary, K., Fichtinger, G., Forestier, G., Gibaud, B., Grantcharov, T.P., Hashizume, M., Heckmann-Nötzel, D., Kennigott, H.G., Kikinis, R., Mündermann, L., Navab, N., Onogur, S., Roß, T., Sznitman, R., Taylor, R.H., Tizabi, M.D., Wagner, M., Hager, G.D., Neumuth, T., Padoy, N., Collins, J., Gockel, I., Goedeke, J., Hashimoto, D.A., Joyeux, L., Lam, K., Leff, D.R., Madani, A., Marcus, H.J., Meireles, O.R., Seitel, A., Teber, D., Ückert, F., Müller-Stich, B.P., Jannin, P., Speidel, S., 2022. Surgical data science - from concepts toward clinical translation. *Medical Image Anal.* 76, 102306. URL: <https://doi.org/10.1016/j.media.2021.102306>, doi:10.1016/j.media.2021.102306.
- Maier-Hein, L., Vedula, S., Speidel, S., Navab, N., Kikinis, R., Park, A., Eisenmann, M., Feussner, H., Forestier, G., Giannarou, S., Hashizume, M., Katić, D., Kennigott, H., Kranzfelder, M., Malpani, A., März, K., Neumuth, T., Padoy, N., Pugh, C., Jannin, P., 2017. Surgical data science for next-generation interventions. *Nature Biomedical Engineering* 1. doi:10.1038/s41551-017-0132-7.
- McMahan, B., Moore, E., Ramage, D., Hampson, S., y Arcas, B.A., 2017. Communication-efficient learning of deep networks from decentralized data, in: *Artificial intelligence and statistics*, PMLR. pp. 1273–1282.
- Micikevicius, P., Narang, S., Alben, J., Diamos, G., Elsen, E., Garcia, D., Ginsburg, B., Houston, M., Kuchaiev, O., Venkatesh, G., et al., 2017. Mixed precision training. *arXiv preprint arXiv:1710.03740*.
- Misra, I., Maaten, L.v.d., 2020. Self-supervised learning of pretext-invariant representations, in: *Proceedings of the IEEE/CVF Conference on Computer Vision and Pattern Recognition*, pp. 6707–6717.
- Misra, I., Zitnick, C.L., Hebert, M., 2016. Shuffle and learn: Unsupervised learning using temporal order verification, in: Leibe, B., Matas, J., Sebe, N., Welling, M. (Eds.), *Computer Vision - ECCV 2016 - 14th European Conference, Amsterdam, The Netherlands, October 11-14, 2016, Proceedings, Part I*, Springer. pp. 527–544. URL: https://doi.org/10.1007/978-3-319-46448-0_32, doi:10.1007/978-3-319-46448-0_32.
- Noroozi, M., Favaro, P., 2016. Unsupervised learning of visual representations by solving jigsaw puzzles, in: *European conference on computer vision*, Springer. pp. 69–84.
- Nwoye, C.I., Mutter, D., Marescaux, J., Padoy, N., 2019. Weakly supervised convolutional lstm approach for tool tracking in laparoscopic videos. *International journal of computer assisted radiology and surgery* 14, 1059–1067.
- Van den Oord, A., Li, Y., Vinyals, O., 2018. Representation learning with contrastive predictive coding. *arXiv e-prints*, arXiv:1807.03748.
- Oord, A.v.d., Li, Y., Vinyals, O., 2018. Representation learning with contrastive predictive coding. *arXiv preprint arXiv:1807.03748*.
- Padoy, N., Blum, T., Ahmadi, S., Feußner, H., Berger, M., Navab, N., 2012. Statistical modeling and recognition of surgical workflow. *Medical Image Anal.* 16, 632–641. URL: <https://doi.org/10.1016/j.media.2010.10.001>, doi:10.1016/j.media.2010.10.001.
- Pan, T., Song, Y., Yang, T., Jiang, W., Liu, W., 2021. Videomoco: Contrastive video representation learning with temporally adversarial examples, in: *IEEE Conference on Computer Vision and Pattern Recognition, CVPR 2021, virtual, June 19-25, 2021*, Computer Vision Foundation / IEEE. pp. 11205–11214. URL: https://openaccess.thecvf.com/content/CVPR2021/html/Pan_VideoMoCo_Contrastive_Video_Representation_Learning_With_Temporally_Adversarial_Examples_CVPR_2021_paper.html.
- Pathak, D., Girshick, R.B., Dollár, P., Darrell, T., Hariharan, B., 2017. Learning features by watching objects move, in: *2017 IEEE Conference on Computer Vision and Pattern Recognition, CVPR 2017, Honolulu, HI, USA, July 21-26, 2017*, IEEE Computer Society. pp. 6024–6033. URL: <https://doi.org/10.1109/CVPR.2017.638>, doi:10.1109/CVPR.2017.638.
- Pathak, D., Krähenbühl, P., Donahue, J., Darrell, T., Efros, A.A., 2016. Context encoders: Feature learning by inpainting, in: *2016 IEEE Conference on Computer Vision and Pattern Recognition, CVPR 2016, Las Vegas, NV, USA, June 27-30, 2016*, IEEE Computer Society. pp. 2536–2544. URL: <https://doi.org/10.1109/CVPR.2016.278>, doi:10.1109/CVPR.2016.278.
- Peng, C., Xiao, T., Li, Z., Jiang, Y., Zhang, X., Jia, K., Yu, G., Sun, J., 2018. Megdet: A large mini-batch object detector, in: *Proceedings of the IEEE*

- conference on Computer Vision and Pattern Recognition, pp. 6181–6189.
- Qian, R., Meng, T., Gong, B., Yang, M., Wang, H., Belongie, S.J., Cui, Y., 2021. Spatiotemporal contrastive video representation learning, in: IEEE Conference on Computer Vision and Pattern Recognition, CVPR 2021, virtual, June 19-25, 2021, Computer Vision Foundation / IEEE. pp. 6964–6974. URL: https://openaccess.thecvf.com/content/CVPR2021/html/Qian_Spatiotemporal_Contrastive_Video_Representation_Learning_CVPR_2021_paper.html.
- Ross, T., Zimmerer, D., Vemuri, A., Isensee, F., Wiesenfarth, M., Bodenstedt, S., Both, F., Kessler, P., Wagner, M., Müller, B., et al., 2018. Exploiting the potential of unlabeled endoscopic video data with self-supervised learning. *International journal of computer assisted radiology and surgery* 13, 925–933.
- Sestini, L., Rosa, B., De Momi, E., Ferrigno, G., Padoy, N., 2021. A kinematic bottleneck approach for pose regression of flexible surgical instruments directly from images. *IEEE Robotics and Automation Letters* 6, 2938–2945.
- Shi, X., Jin, Y., Dou, Q., Heng, P., 2021. Semi-supervised learning with progressive unlabeled data excavation for label-efficient surgical workflow recognition. *Medical Image Anal.* 73, 102158. URL: <https://doi.org/10.1016/j.media.2021.102158>, doi:10.1016/j.media.2021.102158.
- Soomro, K., Zamir, A.R., Shah, M., 2012. UCF101: A dataset of 101 human actions classes from videos in the wild. *CoRR abs/1212.0402*. URL: <http://arxiv.org/abs/1212.0402>, arXiv:1212.0402.
- Tian, Y., Krishnan, D., Isola, P., 2020. Contrastive multiview coding, in: *Computer Vision—ECCV 2020: 16th European Conference, Glasgow, UK, August 23–28, 2020, Proceedings, Part XI 16*, Springer. pp. 776–794.
- Twinanda, A.P., Mutter, D., Marescaux, J., Mathelin, M., Padoy, N., 2016a. Single- and multi-task architecture for surgical workflow at m2cai 2016. arXiv: Computer Vision and Pattern Recognition .
- Twinanda, A.P., Shehata, S., Mutter, D., Marescaux, J., De Mathelin, M., Padoy, N., 2016b. Endonet: a deep architecture for recognition tasks on laparoscopic videos. *IEEE transactions on medical imaging* 36, 86–97.
- Vondrick, C., Shrivastava, A., Fathi, A., Guadarrama, S., Murphy, K., 2018. Tracking emerges by coloring videos, in: Ferrari, V., Hebert, M., Sminchisescu, C., Weiss, Y. (Eds.), *Computer Vision - ECCV 2018 - 15th European Conference, Munich, Germany, September 8-14, 2018, Proceedings, Part XIII*, Springer. pp. 402–419. URL: https://doi.org/10.1007/978-3-030-01261-8_24, doi:10.1007/978-3-030-01261-8_24.
- Wang, X., Jabri, A., Efros, A.A., 2019. Learning correspondence from the cycle-consistency of time, in: *IEEE Conference on Computer Vision and Pattern Recognition, CVPR 2019, Long Beach, CA, USA, June 16-20, 2019, Computer Vision Foundation / IEEE*. pp. 2566–2576. URL: http://openaccess.thecvf.com/content_CVPR_2019/html/Wang_Learning_Correspondence_From_the_Cycle-Consistency_of_Time_CVPR_2019_paper.html, doi:10.1109/CVPR.2019.00267.
- Wu, Z., Xiong, Y., Yu, S.X., Lin, D., 2018. Unsupervised feature learning via non-parametric instance discrimination, in: *Proceedings of the IEEE conference on computer vision and pattern recognition*, pp. 3733–3742.
- Xiao, T., Wang, X., Efros, A.A., Darrell, T., 2020. What should not be contrastive in contrastive learning, in: *International Conference on Learning Representations*.
- Xu, D., Xiao, J., Zhao, Z., Shao, J., Xie, D., Zhuang, Y., 2019. Self-supervised spatiotemporal learning via video clip order prediction, in: *IEEE Conference on Computer Vision and Pattern Recognition, CVPR 2019, Long Beach, CA, USA, June 16-20, 2019, Computer Vision Foundation / IEEE*. pp. 10334–10343. URL: http://openaccess.thecvf.com/content_CVPR_2019/html/Xu_Self-Supervised_Spatiotemporal_Learning_via_Video_Clip_Order_Prediction_CVPR_2019_paper.html, doi:10.1109/CVPR.2019.01058.
- Yang, H., Kahrs, L.A., 2021. Real-time coarse-to-fine depth estimation on stereo endoscopic images with self-supervised learning, in: *2021 IEEE 18th International Symposium on Biomedical Imaging (ISBI)*, IEEE. pp. 733–737.
- Yengera, G., Mutter, D., Marescaux, J., Padoy, N., 2018. Less is more: Surgical phase recognition with less annotations through self-supervised pre-training of cnn-lstm networks. arXiv preprint arXiv:1805.08569 .
- You, Y., Gitman, I., Ginsburg, B., 2017. Large batch training of convolutional networks. arXiv preprint arXiv:1708.03888 .
- Zhang, R., Isola, P., Efros, A.A., 2016. Colorful image colorization, in: *European conference on computer vision*, Springer. pp. 649–666.
- Zhang, R., Isola, P., Efros, A.A., 2017. Split-brain autoencoders: Unsupervised learning by cross-channel prediction, in: *Proceedings of the IEEE Conference on Computer Vision and Pattern Recognition*, pp. 1058–1067.
- Zhuang, C., Zhai, A.L., Yamins, D., 2019. Local aggregation for unsupervised learning of visual embeddings, in: *Proceedings of the IEEE/CVF International Conference on Computer Vision*, pp. 6002–6012.

Dissecting Self-Supervised Learning Methods for Surgical Computer Vision

=====*Supplementary Material*=====

Appendix A. Implementation details

i. Training: Self-supervised pre-training

We use ResNet-50 (He et al., 2016) as the base encoder architecture and 3-layer multilayer perceptron (MLP) as the projection head for all the Self-supervised methods. The projection head uses 2 hidden layers (2048, 256) including ReLU activation and batch normalization with input layer dimension of size 2048 and output layer dimension of size 4096. Specific implementation details for each method are as follows: *MoCo* v2 uses a queue of size 65536 with a decay parameter (λ) of 0.999 and temperature (τ) of 0.2; *SimCLR* uses the temperature (τ) of 0.1; *SwAV* uses 3 Sinkhorn-Knopp iterations and regularization parameter of 0.05; *DINO* uses decay parameter (λ) of 0.996, warm-up iterations 7500, and centering decay parameter λ_c of 0.9.

We conduct all the self-supervised training experiments on four V100 GPUs using SGD optimizer with LARC (You et al., 2017) (“trust” coefficient $\eta = 0.001$), base learning rate of 0.1, weight decay of 0.000001, and momentum of 0.9. The batch size is set to 64/GPU (256 total batch size) except in the **Batch size** hyperparameter study where we use batches of size 128 (32/GPU), 256 (64/GPU), 512 (128/GPU) and 1024 (256/GPU). We use the VISSL framework⁵ to run all the experiments using synchronized batch normalization (Peng et al., 2018) and automatic mixed precision (AMP) (Micikevicius et al., 2017).

For the **Initialization** hyperparameter study, we initialize ResNet-50 weights as follows: 1) fully-supervised imagenet weights (“FS”) from torchvision⁶, 2) self-supervised imagenet weights (“SS”) for SimCLR from VISSL⁷, for MoCo v2 from their Github repo⁸, for SwAV from VISSL⁹, and for DINO from their Github repo¹⁰.

ii. Training: Downstream tasks

Hyperparameter study: in all the experiments (Section. 3.3), after the self-supervised training, the trunk of the encoder is frozen and the SSL head is replaced by a linear head that maps the feature vector (2048) to the number of outputs for the relevant task. The linear layer is trained on 1 GPU using an SGD optimizer with a base learning rate of 3e-3 and 1e-1 for phase recognition and tool presence detection, respectively. The layer is trained for 30 epochs for phase with a step-wise learning rate decay of 0.3 (milestone: 15 epoch) and 50 epochs for tool with a step-wise learning rate decay of 0.1 (milestones: 20, 30 and 40 epoch). Frames are sampled at 1 fps for the linear evaluation described above.

Phase recognition is formulated as a multi-class classification problem where a weighted cross-entropy loss is minimized. The class weights for phases is computed using median frequency balancing (Eigen and Fergus, 2015) on the training set.

Since tool presence detection is a multi-label classification problem, we employ weighted binary cross-entropy loss:

$$L = \sum_{c=1}^C \frac{-1}{N} (W_c y_c \log(\sigma(\hat{y}_c)) + (1 - y_c) \log(\sigma(\hat{y}_c))), \quad (\text{A.1})$$

where y_c is the ground truth tool presence label for class c , \hat{y}_c is the predicted probability for class c , and W_c is the class weight.

Data supply study: in the data supply study (Section 3.4), after the SSL training, we follow a similar downstream training setup to the one mentioned above, where we replace the SSL head with a linear layer. However, we train the full model for downstream tasks without freezing the encoder’s trunk. For the task of phase recognition, all the experiments are trained on 4 GPUs using SGD optimizer with LARC (You et al., 2017) for 30 epochs. Further, we use augmentations and train the model using a cross-entropy loss. When training the temporal model, the TCN is trained on the features extracted after the phase finetuning using an Adam optimizer (Kingma and Ba, 2014) for 100 epochs with a base learning rate of 3e-3 and a learning rate decay of 3e-1 (milestone: 75 epoch). Frames are sampled at 1 fps for the linear finetuning and TCN training described above.

Experiments involving tool presence detection, the models are trained on 4 GPUs using an Adam optimizer for 50 epochs with a base learning rate of 1e-5 and learning rate decay of 0.1 (milestone: 25 epoch). As specified above, we use weighted binary

⁵<https://github.com/facebookresearch/vissl>

⁶<https://download.pytorch.org/models/resnet50-0676ba61.pth>

⁷https://dl.fbaipublicfiles.com/vissl/model_zoo/simclr_rn50_800ep_simclr_8node_resnet_16_07_20_7e8feed1/model_final_checkpoint_phase799.torch

⁸https://dl.fbaipublicfiles.com/moco/moco_checkpoints/moco_v2_800ep/moco_v2_800ep_pretrain.pth.tar

⁹https://dl.fbaipublicfiles.com/vissl/model_zoo/swav_in1k_rn50_800ep_swav_8node_resnet_27_07_20_a0a6b676/model_final_checkpoint_phase799.torch

¹⁰https://dl.fbaipublicfiles.com/dino/dino_resnet50_pretrain/dino_resnet50_pretrain.pth

cross-entropy loss with the class weights computed using inverse frequency balancing for different percentages and samples of the training data used.

All the above training setting is employed when training models with 100% of the labelled data. In lower labelled data settings, the number of epochs and milestones are scaled inversely in proportion with the percentage of training data. This provides the models with similar number of updates irrespective of the amount of labeled data available.

Appendix B. Augmentation details

Table B.7 shows the details of all the augmentations used for the self-supervised pre-training and supervised fine-tuning experiments.

Table B.7. Different image augmentations used in the self-supervised pre-training and supervised fine-tuning experiments. The Source “RA” uses the RandAugment (Cubuk et al., 2020b) implementations that randomly selects two augmentations from the list and applies the augmentation with a given probability ($prob$), magnitude (M), and standard deviation on the magnitude (M_σ). The source “torchvision” uses the torchvision implementation for Random-erasing, Horizontal-flip, and Multi-crop augmentations.

	Name	Source	Parameters
Color	Sharpness	RA	$prob = 0.5, M = 8.0, M_\sigma = 0.5$
	Brightness	RA	$prob = 0.5, M = 8.0, M_\sigma = 0.5$
	Contrast	RA	$prob = 0.5, M = 8.0, M_\sigma = 0.5$
	Color	RA	$prob = 0.5, M = 8.0, M_\sigma = 0.5$
	Auto-contrast	RA	$prob = 0.5, M = 8.0, M_\sigma = 0.5$
	Equalize	RA	$prob = 0.5, M = 8.0, M_\sigma = 0.5$
	Random-erasing	torchvision	$prob = 0.8, scale = [0.02, 0.1]$
Geometric	Rotate	RA	$prob = 0.5, M = 8.0, M_\sigma = 0.5$
	Translate-x	RA	$prob = 0.5, M = 8.0, M_\sigma = 0.5$
	Translate-y	RA	$prob = 0.5, M = 8.0, M_\sigma = 0.5$
	Shear-x	RA	$prob = 0.5, M = 8.0, M_\sigma = 0.5$
	Shear-y	RA	$prob = 0.5, M = 8.0, M_\sigma = 0.5$
	Horizontal-flip	torchvision	$prob = 0.5$
Strong Color	Posterize	RA	$prob = 0.5, M = 8.0, M_\sigma = 0.5$
	Solarize	RA	$prob = 0.5, M = 8.0, M_\sigma = 0.5$
	inversion	RA	$prob = 0.5, M = 8.0, M_\sigma = 0.5$
Multi Crop	MC2: multi-crop 2	torchvision	$224 \times 224 = 2, scale = [0.5, 1]$
	MC2: multi-crop 4	torchvision	$(224 \times 224 = 2), (96 \times 96 = 2), scale = [0.5, 1]$
	MC2: multi-crop 8	torchvision	$(224 \times 224 = 2), (96 \times 96 = 6), scale = [0.5, 1]$